Fundamental law underlying predictive remapping

Ifedayo-EmmanuEL Adeyefa-Olasupo*
HHMI Janelia Research Campus, Ashburn, Virginia 20147, USA;
Department of Psychiatry, Charité—Universitätsmedizin Berlin, 10117 Berlin, Germany;
and Berlin School of Mind and Brain, Humboldt-Universitat zu Berlin, 10099 Berlin, Germany

(Received 24 October 2022; accepted 13 March 2023; published 29 March 2023)

This article is part of the Physical Review Research collection titled Physics of Neuroscience.

Predictive remapping (P_{RE})—the ability of cells in retinotopic brain structures to transiently exhibit spatiotemporal shifts beyond the spatial extent of their classical anatomical receptive fields—has been proposed as a primary mechanism that stabilizes an organism's percept of the visual world around the time of a saccadic eye movement. Despite the well-documented effects of P_{RE}, a biologically plausible mathematical framework that specifies a fundamental law and the functional neural architecture that actively mediates this ubiquitous phenomenon does not exist. We introduce the Newtonian model of P_{RE}, where each modular component of P_{RE} manifests as three temporally overlapping forces: centripetal ($\vec{f_C}$), convergent ($\vec{f_P}$), and translational ($\vec{f_T}$), that perturb retinotopic cells from their equilibrium extent. The resultant and transient influences of these forces $\vec{f_C} + \vec{f_P} + \vec{f_T}$ gives rise to a neuronal force field that governs the spatiotemporal dynamics of P_{RE}. This neuronal force field fundamentally obeys an inverse-distance law $P_{RE} \propto \frac{1}{r^{1.6}}$, akin to Newton's law of universal gravitation [I. Newton, *Newton's Principia: The Mathematical Principles of Natural Philosophy* (Geo. P. Putnam, New-York, 1850)] and activates retinotopic elastic fields elφ's. We posit that elφ's are transient functional neural structures that are self-generated by visual systems during active vision and approximate the sloppiness (or degrees of spatial freedom) within which receptive fields are allowed to shift, while ensuring that retinotopic organization does not collapse. The predictions of this general model are borne out by the spatiotemporal changes in visual sensitivity to probe stimuli in human subjects around the time of an eye movement and qualitatively match neural sensitivity signatures associated with predictive shifts in the receptive fields of cells in premotor and higher-order retinotopic brain structures. The introduction of this general model opens the search for possible biophysical implementations and provides experimentalists with a simple, elegant, yet powerful mathematical framework they can now use to generate experimentally testable predictions across a range of biological systems.

DOI: 10.1103/PhysRevResearch.5.013214

I. INTRODUCTION

Biological systems can be classified into two distinct groups: foveated and afoveated systems. In foveated systems (e.g., humans, rhesus macaques, great apes), the central 2° of visual space is extensively represented in the retina (with the highest cone photoreceptor density in the fovea) or premotor and primary visual brain structures. Afoveated systems, on the other hand (e.g., rodents, fruit flies, zebrafish), do not possess a fovea or premotor and primary visual brain structures that magnify the representation of a specific region in visual space. This in turn equips afoveated systems with the unique ability to coarsely represent a wider field of view at a single point in time. Despite the structural differences between foveated and afoveated systems, directed saccadic eye movements are routinely recruited by both biological systems [1–5]. Saccades can bring a new stimulus of interest (e.g., camouflaged prey, encroaching predator) that is sampled on the peripheral retina or located outside of the organism's visual field into a region that allows for the rapid identification and detailed inspection of the new stimulus [3,6].

Saccadic eye movements cause large and rapid displacements of the retinal image. These displacements introduce significant retinal disruptions, akin to those observed when attempting to photograph a rapidly moving stimulus using a camera. Indeed, different visual systems have evolved to account for these sudden retinal image disruptions such that their gaze is quickly stabilized, and their perception of the visual world remains relatively continuous [7–10]. The ability of a visual system in general to account for these incessant retinal disruptions is commonly referred to as perceptual (or spatial) constancy [11–15].

Translational remapping—the ability of cells within retinotopic brain structures to predictively shift their neural sensitivity beyond the spatial extent of their classical anatomical receptive fields to their future postsaccadic locations just before saccade onset—has been proposed as a primary mechanism that mediates spatial constancy [Fig. 1(a)] [16–19]. However, more recent electrophysiological studies in foveated

*adeyefaolasupoi@janelia.hhmi.org

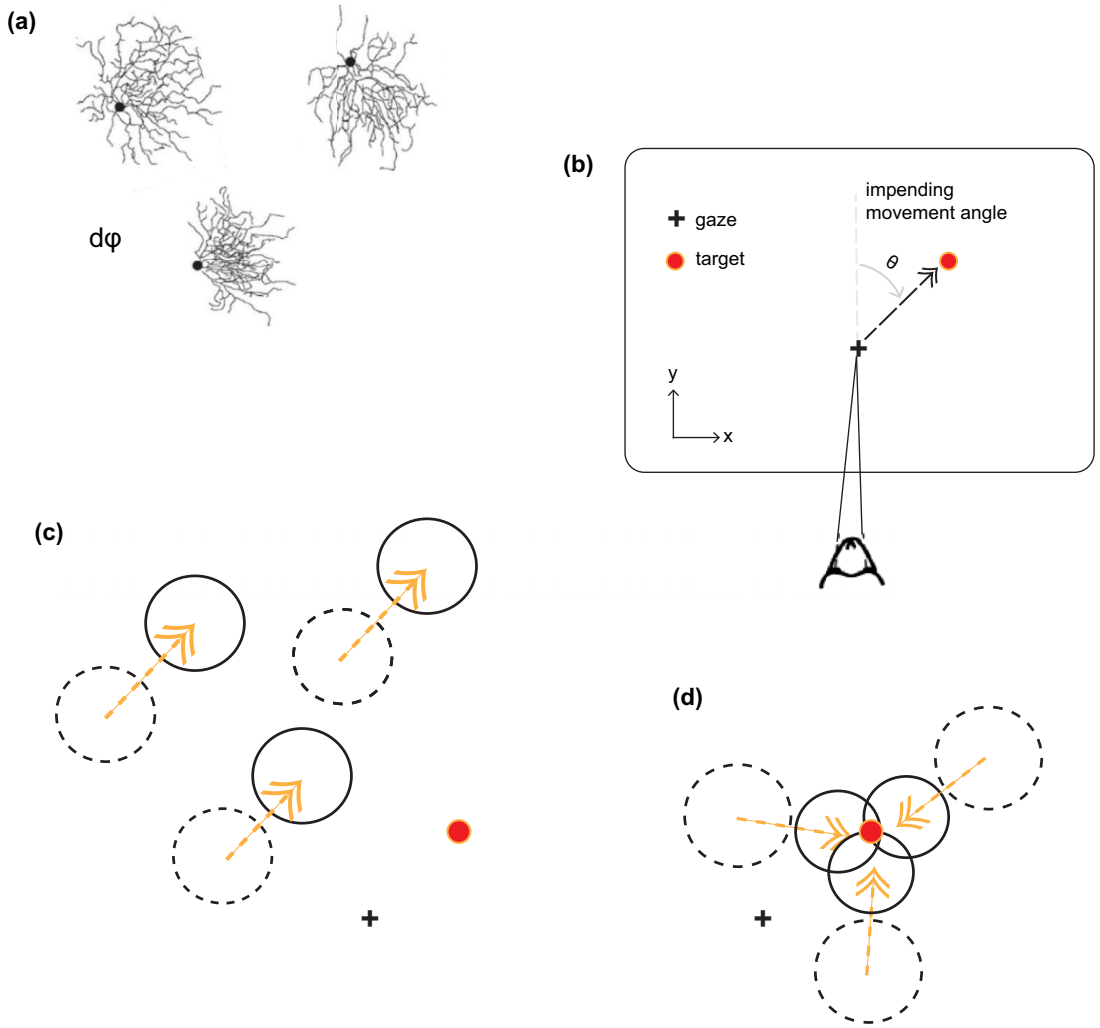

FIG. 1. Translational vs the convergent form of predictive remapping. (a) Cartoon of three visual cells in a dendritic field ($d\varphi$). A best-fit contour that includes the center of the cell and dendritic extent is referred to as the anatomical classical receptive field (cRF) of the cell (see Ref. [50]). (b) Cartoon of an animal attending to a region within its visual field and preparing to make a saccadic eye movement (i.e., black dotted arrow) toward an ecologically relevant visual stimulus (red dot). (c) According to the translational form of predictive remapping, cRFs (i.e., dotted black circles) do not respond when a presaccadic flashed probe (e.g., Gabor probe) is placed within these extents just before the saccade is made. Instead, they respond when the flash occurs within their future postsaccadic locations (i.e., solid circles representing neighboring cRFs). This extent is roughly proportional to the magnitude of the impending saccadic eye movement vector. (d) According to the convergent form of remapping, the region around the target constitutes where neural sensitivity and, as a result, visual sensitivity will be the highest, as if cRFs have converged toward and around the preselected visual stimulus.

and afoveated systems have challenged this dominant view of predictive remapping (P_{RE}) and have instead demonstrated that these transient predictive shifts are directed toward (i.e., along the known trajectory that aligns with a target of interest) and/or around a preselected peripheral site which includes the spatial extent of the target [Fig. 1(b)]. This form of P_{RE} in the foveated literature is referred to as convergent remapping [20–23].

Translational and convergent accounts of P_{RE} thus remain at odds, and the functional role that these divergent forms of transient receptive field shifts play in mediating spatial constancy is vigorously debated [24–27]. For example, prior studies have routinely sampled regions in visual space that yield results favorable to one form of P_{RE} over another. In fact, with an unbiased spatial sampling, a more recent study suggests that the functional correlates of convergent remapping may include additional components [28], an account that contradicts earlier results regarding the functional correlates of P_{RE} [29,30]. In addition to this, the only study that did increase spatial sampling around a preselected peripheral site was devoid of a computational framework to correctly contextualize and interpret reported observations [31]. It is therefore not surprising that the observations from that study are radically inconsistent with well-established classical neurophysiological accounts of P_{RE} [16–19].

Equally unresolved is the issue of time. First, most studies have only assessed the consequences of P_{RE} on visual and neural sensitivity within a limited presaccadic window (e.g., −250 to +50 ms with respect to the onset of a saccadic eye movement). To this end, it is unclear how

transient receptive field shifts that occur within much earlier presaccadic windows actively modulate perisaccadic and postsaccadic sensitivity [27]. Finally, a recent study has reported that P_{RE} includes a translational component followed by a convergent component, with each component specified within distinct nonoverlapping temporal windows [32,33]. This temporal account of P_{RE} is, however, at odds with the canonical order of presaccadic events [15], and a more recent study has challenged these results on methodological grounds [22].

In addition to these unresolved issues, there are three important questions about the visuomotor system previous investigations have overlooked. First, the frequency of saccades (∼2–4 times per second) [34] and the accompanying predictive receptive field shifts can be energetically expensive [35], yet a fundamental law visual systems in general use to balance energy costs with predictive function remains a mystery. Second, the functional neural architecture that supports increased or sustained sensitivity of retinotopic cells beyond their anatomical classic center-surround structure, while preventing radical and unsustainable forms of remapping (e.g., overconvergence or overtranslation), is unknown. Finally, no computational investigations of P_{RE} have been able to provide an explanation as to how the visual system ensures the immediate availability of neural sensitivity at the future postsaccadic location of the saccade target [36]. This rapid availability of neural sensitivity which directly supports visual sensitivity on the behavioral domain cannot be explained by pure translational or convergent shifts.

To provide an account for (a) the spatiotemporal characteristics that define P_{RE}, (b) a fundamental law and the functional neural architecture which ensures that retinotopic cells are appropriately sensitized toward different loci in visual space, while preserving retinotopic organization around the time of a saccadic eye movement, and (c) the jump in late presaccadic sensitivity in the periphery and the immediate availability of postsaccadic sensitivity at the future center of gaze, we developed a simple, elegant, yet powerful general model of P_{RE} derived using Newtonian mechanics. Next, we simulated changes in population neural density. We assume that changes in density levels are equivalent to the changes in neural sensitivity levels reported in previous neurophysiological studies. We further assume that these neural sensitivity changes fundamentally shape visual sensitivity levels within distinct retinotopic regions of visual space (i.e., foveal, parafoveal, and peripheral extents) [21,22,31]. We later used these changes in density levels to assess the extent they could either predict or qualitatively match functional and neurophysiological readouts in the extant literature. Finally, to directly assess the generalizability and biological plausibility of the model, we conducted three psychophysics experiments. These experiments directly investigated the transient consequences of P_{RE} on visual sensitivity to flashed visual probe stimuli in human subjects within foveal, parafoveal, and peripheral extents of visual space, and a larger presaccadic and postsaccadic window ($-\sim$600 to $+$ 150 ms), results which we later compared with simulated results. Comparisons between experimental and simulated results were followed by rhythmic investigations we used to further scrutinize a core assumption of the model.

II. MODEL

Since the initial discovery of P_{RE} ∼45 years ago [37], an assortment of models has attempted to specify a biophysical mechanism, a specific retinotopic brain structure, and/or a neural circuit underlying this ubiquitous phenomenon [38–43]. Models that opted for a less reductionist approach were carefully parametrized and/or included nonmodular components, with simulations ultimately conforming to an experimental demand (i.e., one form of remapping over another or the combination of both) [44–46]. Indeed, these approaches, as recent reviews demonstrate [24,25] have fundamentally obscured the emergent simplicity and elegance of the phenomenon [47].

Acutely aware of the pitfalls previous models have been unable to avoid, the proposed model at present is a mathematical abstraction. By definition, such abstraction is agnostic to a specific biophysical mechanism, a specific retinotopic brain structure, or a specific neural circuitry. The proposed model is also not beholden to specific experimental demands and, unlike previous models, is motivated by previous experimental observations in foveated and afoveated biological systems.

The principal functional unit of the proposed model is retinotopic cells. These cells subserve retinotopic brain structures and receive either direct or indirect inputs from the retina. We will refer to the excitatory extent of these units as retinotopic receptive fields RF_i's (Fig. 2). Across different retinotopic brain structures in foveated and afoveated biological systems, RF_i's modulate changes in neural sensitivity across visual space. These changes directly shape levels of visual sensitivity at a location in visual space the organism is currently attending to (i.e., its current center of gaze) as well as intermediate and peripheral extents from this current center point.

An RF_i is characterized by two principal parameters: (a) c_i, the central location of the RF_i $(x_0,\ y_0)$ at t_0 (when a visual system is at an equilibrium state) [Figs. 2(a) and 2(c)]. Here, c_i determines the eccentricity (ecc_i) of the RF_i, that is, the spatial extent of the RF_i with respect to the current center of gaze, and (b) $r\alpha_i$, the radius of the RF_i in a foveated system, which is dependent on ecc_i and k, where ε_0 is defined as the radius of the RF_i at an ecc ~ 0 [Eq. (2)], or $r\beta_i$, the radius of the RF_i in an afoveated system, where ε_1 does not scale with ecc_i [Eq. (2)]:

$$r\alpha = k\mathrm{ecc} + \varepsilon_0, \tag{1}$$

$$r\beta = 0 + \varepsilon_1. \tag{2}$$

Traditionally, RF_i's are thought to be constrained by their anatomical receptive field [48,49]. Here, however, we posit that the anatomical receptive field of an RF_i and its functional counterpart do not share a one-to-one mapping [50], specifically around the time of a saccadic eye movement [1,16–29,51]. To this end, we further posit that RF_i's fundamentally behave like spring-loaded sensors [4] that can undergo transient spatiotemporal contortions, consistent with the translational and convergent forms of P_{RE} [16–22], and RF_i dynamics that have been observed across afoveated biological systems [23,52,53]. The proposed model assumes that there are limits to which RF_i's can transiently contort

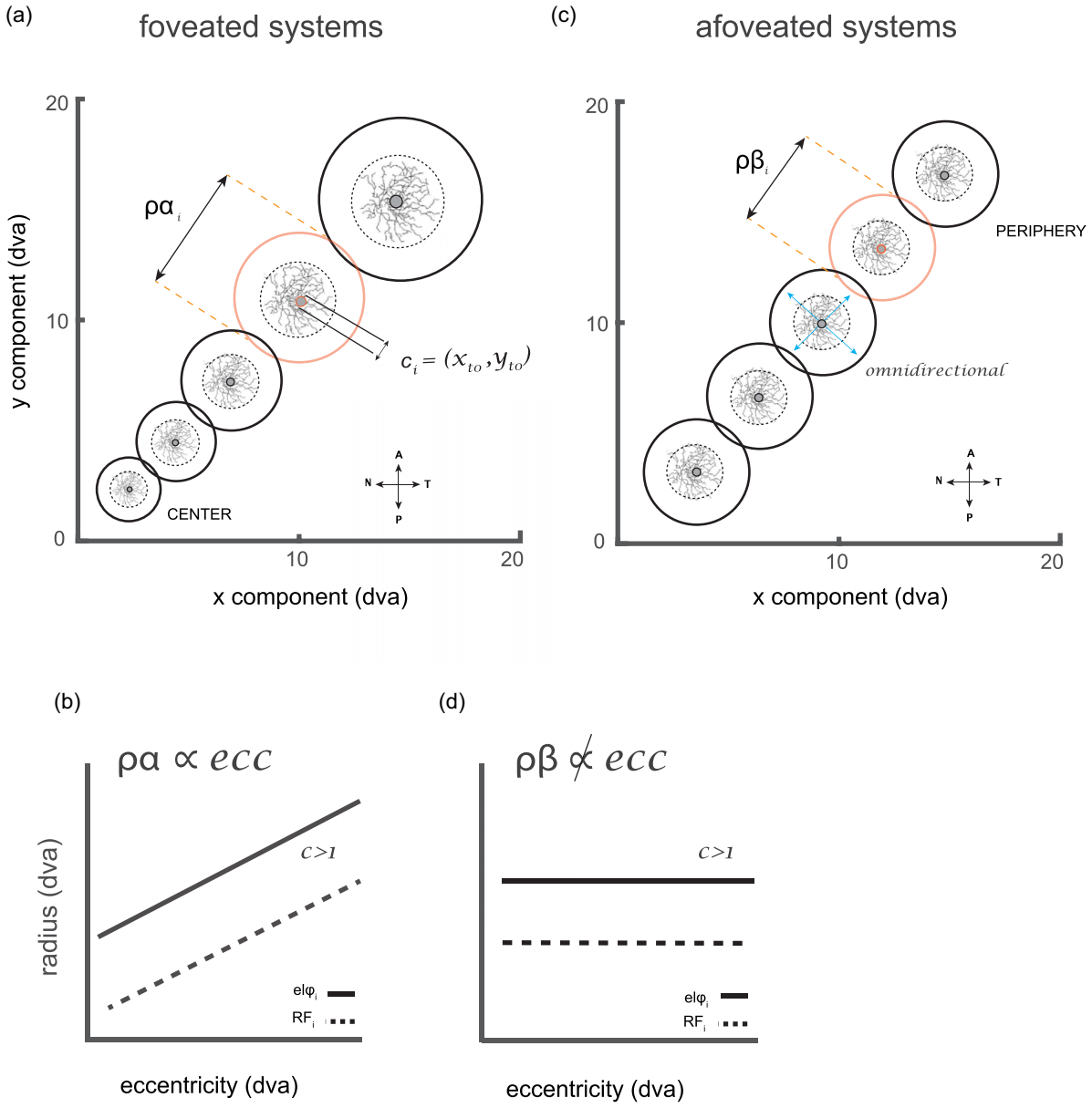

FIG. 2. Proposed putative functional neural architecture that supports active vision. For every receptive field (RF_i), there is an elastic field ($el\varphi_i$). Here, titling of overlapping $el\varphi$'s along a ∼45° extent in a visual field is shown for illustration purposes. Under normal conditions, RF_i's and $el\varphi$'s at $t_0 + 1$ tile the entire visual field. Depending on the biological system, RF_i's can either be (a) eccentricity dependent or (c) noneccentricity dependent. N, nasal; A, anterior; T, temporal; and P, posterior. (b) and (d) The radius of RF_i's (in degrees of visual angle) as a function of their distance from the center of visual space (or eccentricity). When RF_i's are multiplied by $c > 1$, the outer functional boundary of $el\varphi$'s will demonstrate a larger radius which allows RF_i's the ability to shift beyond their spatial extent.

within or beyond their classical anatomical receptive fields so that retinotopic organization is always maintained [46]. We therefore extend the idea of the anatomical receptive field of a retinotopic cell by introducing the concept of its functional elastic field ($el\varphi$). Here, $el\varphi$'s are composed of transient outer functional boundaries [depicted as the large orange annulus in Figs. 2(a) and 2(c)] and an inner boundary which roughly aligns with the spatial extent around c_i. We posit that conserved across foveated and afoveated systems is the principle that ρ, the radius of the transient outer functional boundary of a given $el\varphi$, is the product of $r\alpha\beta$ multiplied by c, a constant factor >1 [Eqs. (3)–(5)], Figs. 2(b) and 2(d), and is omnidirectional with respect to the classical extent of the RF_i:

$$\rho = cr\alpha\beta, \tag{3}$$

$$\rho\alpha = \begin{cases} 0, & \text{if } c \text{ is zero} \\ r\alpha, & c = 1 \\ >r\alpha, & c > 1 \end{cases}, \tag{4}$$

$$\rho\beta = \begin{cases} 0, & \text{if } c \text{ is zero} \\ r\beta, & c = 1 \\ >r\beta, & c > 1 \end{cases}. \tag{5}$$

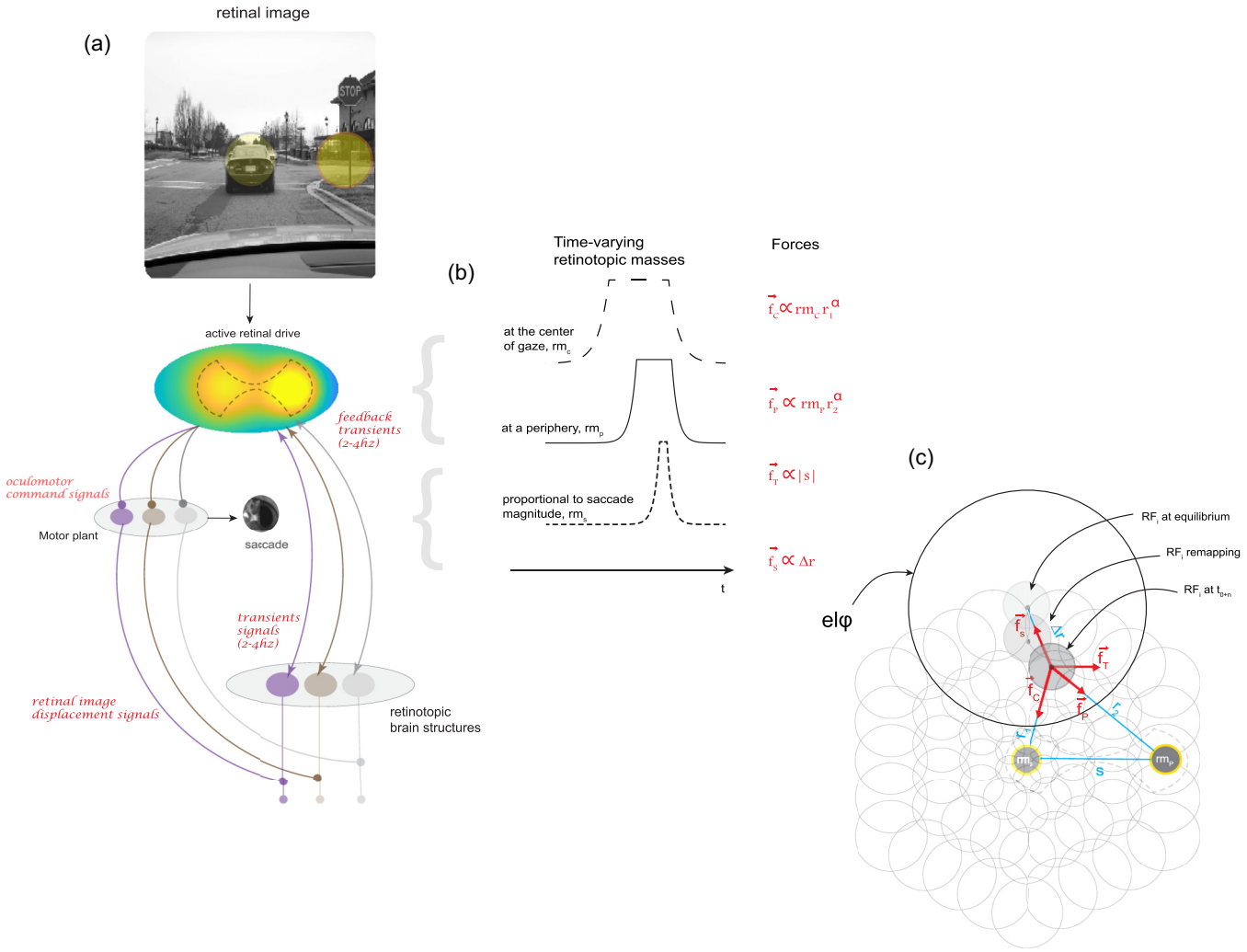

FIG. 3. The physics underlying predictive remapping. (a) The dynamics that underlie attentional-oculomotor signals across retinotopic brain areas is entrained by delta rhythmicity (2–4 Hz). (b) Attentional and oculomotor signals manifest as three principal retinotopic masses. rm_c represents centripetal signals and is modeled as a varying mass located at the center of gaze. rm_p represents convergent signals and is modeled as a varying retinotopic mass located at the peripheral site corresponding to the saccade target. rm_t represents translational signals and is modeled as a virtual retinotopic mass at infinity located in the direction of the impending retinal displacement the saccade will induce. (c) Retinotopic field consisting of population receptive field (RF_i's) that tile foveal, parafoveal, and peripheral regions of visual space perturbed by a force field. A single RF_i and its remapping extent is exaggerated in gray for illustration purposes, while the outer functional boundary of its elastic field (elφ) is depicted in black, also exaggerated for illustration purposes.

Self-generated by visual systems only around the time of an eye movement, elφ's prevent radical and unsustainable forms of P_{RE} (e.g., overtranslation, overconvergence). They also allow an RF_i the ability to undergo transient spatiotemporal shrinking within its anatomical extent, which can enhance the neural representation of small ecologically relevant visual stimuli [20,21,50,54]. Conversely, elφ's can also support transient RF_i stretching and expansions beyond the anatomical limit of an RF_i, consistent with the translational account of P_{RE} [4,16–19,54–56]. Taken together, these transient spatiotemporal shifts manifest as distortions of population neural density [21,22] which temporarily distorts the representation of visual space in general [57–61].

The onset of a retinal image evokes visually transient signals within the retina. These signals are sent to relevant retinotopic brain structures during a detailed inspection of the current stimulus, the selection of a future stimulus, and around the time of a directed or spontaneous saccadic eye movement [62] [Fig. 3(a)]. We use the term *active* to denote the frequency at which these signals are being sent to relevant retinotopic brain structures. The selection and further inspection of a visual stimulus before the execution of a directed or spontaneous saccadic eye movement is marked by an array of visually mediated behavioral dynamics (e.g., small fixational eye movements [63,64], tilting of the head to visually inspect a stimulus [65,66]). These dynamics are supported by delta rhythmicity (2–4 Hz), which is known to predict attentional shifts before a saccadic eye movement in foveated systems [67]. In response to the onset of a visual stimulus or the selection of a new one, in both foveated [37,67–70] and afoveated systems [3,52], a quick burst in neural activity within premotor brain structures occurs. We posit that this quick burst in neural activity is equivalent to oculomotor command signals and made available to retinotopic brain

structures around the time of a saccadic eye movement. We refer to the availability of these signals as *retinal image displacement signals* [Fig. 3(a)]. Retinotopic brain structures go on to use information about the impending displacement of the retinal image to modify persistent incoming visually transient signals originating from the retina. We refer to the modification of these signals as *feedback transient signals*. Because of the omnipresent nature of these retinal image displacement signals [71], we hypothesize these signals along with early and later feedback transient signals (both supported by delta rhythmicity) [67] uniquely equip an RF_i with the ability to perform basic trigonometric operations, that is, estimate from its perspective the direction and magnitude it should shift beyond its classical anatomical extent [72]. We will refer to these early and late feedback transient signals and retinal image displacement signals, in aggregate, as *attentional-oculomotor* signals.

At its core, the proposed model assumes that attentional-oculomotor signals act as forces that perturb spring-loaded RF_i's from their equilibrium positions. We abstract these neurobiologically inspired forces as being exerted by three principal time-varying retinotopic masses $rm(t)$, subtended either at a central (rm_c) or peripheral (rm_p) site in visual space or at infinity (rm_s), whose action is to produce a force in the direction of and parallel to the impending retinal displacement the saccadic eye movement will introduce. We assume that the current (rm_c) or the future (rm_p) location in visual space that is sampled on the retina does not abruptly appear and then disappear akin to a step function but gradually appears and fades [11–15,73]. For this very reason, we modeled each rm_i as a piecewise function [Eqs. (6)–(8)], where rm_i approaches 0 as t remains less than t_{i1}, followed by a gradual growth (ct^i) which is dependent on i, a stable plateau, followed by a gradual decay (ct^{-i}), as i remains >0:

$$rm_c(t) = \begin{cases} 0, & t < t_{x1} \\ c_1 t^n, & t_{x1} < t < t_{x2} \\ \text{const.}, & t_{x2} < t < t_{x3} \\ c_1 t^{-n}, & t_{x3} < t < t_{x4} \\ 0, & t_{x4} < t < t_{x5} \end{cases}, \tag{6}$$

$$rm_p(t) = \begin{cases} 0, & t < t_{y1} \\ c_2 t^m, & t_{y1} < t < t_{y2} \\ \text{const.}, & t_{y2} < t < t_{y3} \\ c_2 t^{-m}, & t_{y3} < t < t_{y4} \\ 0, & t_{y4} < t < t_{y5} \end{cases}, \tag{7}$$

$$rm_s(t) = \begin{cases} 0, & t < t_{z1} \\ c_3 t^p, & t_{z1} < t < t_{z2} \\ \text{const.}, & t_{z2} < t < t_{z3} \\ c_3 t^{-p}, & t_{z3} < t < t_{z4} \\ 0, & t_{z4} < t < t_{z5} \end{cases}, \tag{8}$$

To perturb an RF_i, let $\vec{f}$ be the force that exerts its influence on an RF_i which is the product of rm and $\vec{a_t}$, the acceleration at time t, where rm assumes unit retinotopic mass of RF_i [Eq. (9)]. Here, $\vec{v_t}$ denotes the velocity at time t which is used to compute $\vec{\Delta r}$, the remapping vector for an RF_i from its current position [Eqs. (10) and (11)]. Also, $\vec{p_t}$ denotes the remapping operator which causes an RF_i to displace its extent while being modulated by its elφ, while r_0 denotes the Euclidian distance of the current location of an RF_i from its anatomical extent [Eqs. (12) and (13)]. Taken together, the movement of an RF_i from and back toward its anatomical extent produces retinotopic spatiotemporal trajectory fields Fig. 4:

$$\vec{f} = rm\vec{a_t}, \tag{9}$$

$$\vec{v} = \vec{v_{t-1}} + \vec{a}\,\Delta t, \tag{10}$$

$$\vec{\Delta r} = \vec{v_{t-1}}\Delta t + \tfrac{1}{2}\vec{a}(\Delta t)^2, \tag{11}$$

$$\vec{p_t} = \vec{p_{t-1}} + \vec{\Delta r}, \tag{12}$$

$$r_0 = \sqrt{(p_x - x_0)^2 + (p_y - y_0)^2}. \tag{13}$$

We posit that presaccadic attentional and oculomotor processes manifest in three specific types of forces that temporally align with (a) early visually transient signals originating from the retina, (b) late feedback trainsets that actuate the selection of a peripheral site, and (c) retinal image displacement signals derived from oculomotor motor command signals that impinge on retinotopic brain structures. The proposed model assumes that the transient perturbations of RF_i's, triggered by the linear summation of these forces, are the underlying causes of P_{RE}, Eq. (19). The earliest force—a centripetal one ($\vec{f_C}$) overlapping with the time of early visually transient signals during fixation—causes RF_i's to transiently exhibit centripetal shifts toward the current center of gaze, where kc_α is the centripetal constant, $\vec{U_{rm_C}}$ is the unit vector in the direction of r_1, the spatial difference between RF_i's and rm_C raised to a scalar α, distance (or predictive) exponent [Eq. (14)]. A centripetal force allocates a disproportionate amount of the neural resources of a visual system toward the current center of gaze [62,72,74]. This initial force is followed by a convergent force ($\vec{f_P}$), where kp_α is the convergent constant, $\vec{U_{rm_p}}$ is the unit vector in the direction of r_2, the spatial difference between RF_i's and rm_p raised to a scalar α [Eq. (15)]. The onset of a convergent force precedes impending retinal image displacement signals and causes RF_i's to exhibit convergent shifts toward the periphery. Counter to the dominant intuition in the extant literature [19,20,31], the principal aim of these convergent shifts is not to directly provide peripheral locations with a neural advantage when compared with less peripheral extents but divest intermediate parafoveal RF_i's of the remaining resources they did not initially allocate toward the current center of gaze.

As the organism prepares and plans to execute an impending saccadic eye movement, oculomotor command signals which trigger retinal image displacement signals give rise to a translational force ($\vec{f_T}$), where kt_α is the translational constant, $\vec{U_{rm_S}}$ is the unit vector in the direction of rm_S, while $|s|$ is the magnitude of the impending saccade [Eq. (16)]. Preceding convergent force in combination with the onset of a translational force causes RF_i's to exhibit convergent and translational shifts toward a preselected peripheral site (i.e., jumpstart the allocation of neural resources toward future

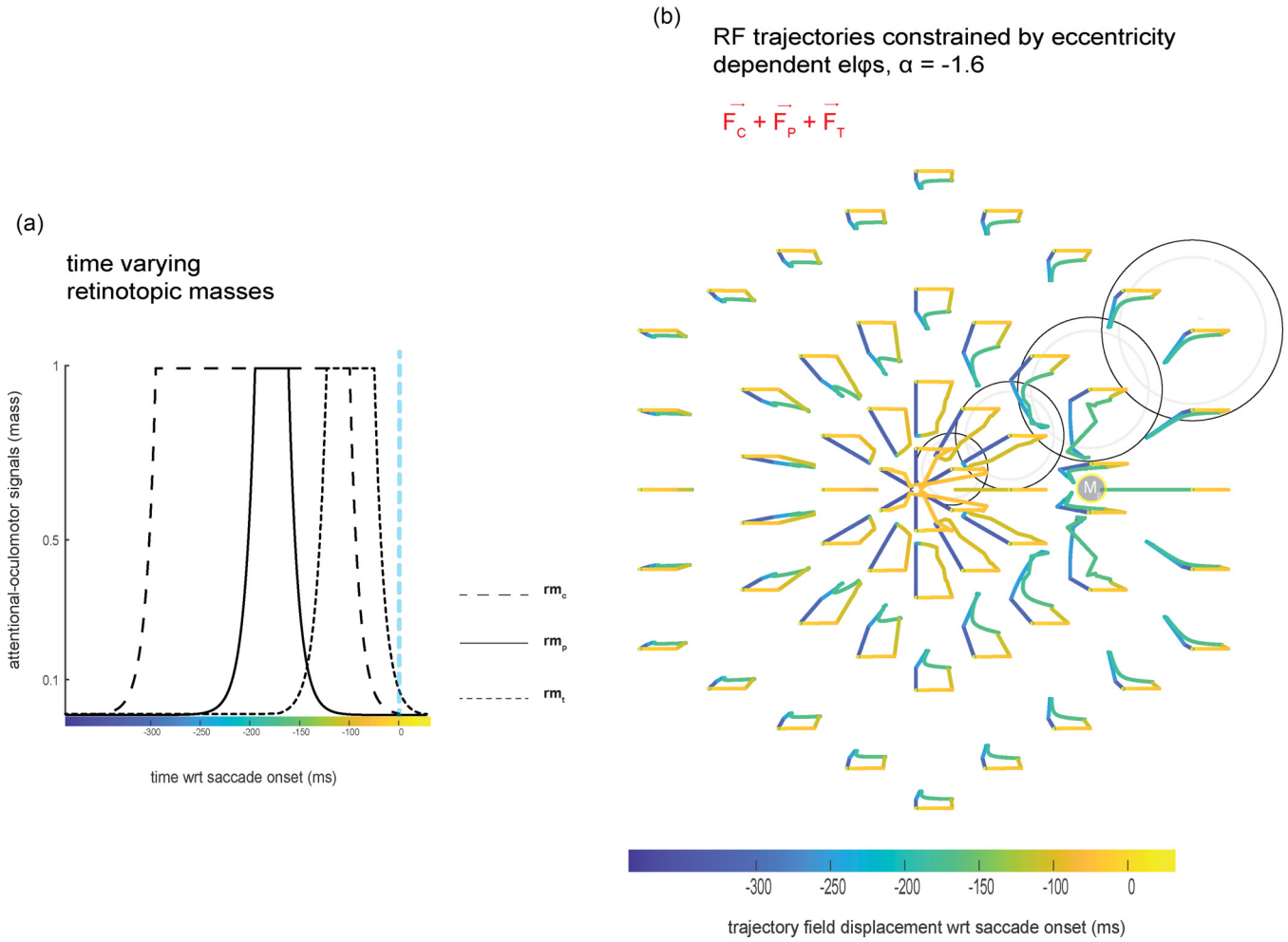

FIG. 4. RF_i shifts under an inverse force field driven by simulated centripetal, convergent, and translational signals. (a) Corresponding time varying masses for the case when RF_i's were perturbed, the linear combination of three types of retinotopic signals modeled as independent forces. The blue dotted line indicates the offset of the centripetal force, which marks the onset of a saccadic eye movement. (b) Spatiotemporal RF_i trajectories starting from the most central point of each RF_i under an inverse force field ($\alpha = -1.6$). Note that each RF_i (light gray) possess an eccentricity-dependent elφ; however, for illustration purposes, only a few are shown (black annulus).

postsaccadic locations) [21]. The growing influence of a translational force and a declining convergent force causes RF_i's to directly jump toward their future postsaccadic locations [18], while a declining centripetal force (i.e., the onset of transient feedbacks) triggers convergent RF_i shifts around a preselected target [20,22]. Finally, it is worth noting that the spring force $\vec{f_S}$ is the product of r_o and k_0, the spring constant [Eq. (17)]. While an elφ ensures that RF_i's approaching their elastic limits are inhibited, $\vec{f_S}$ actuates the offset of each principal force. To obtain k_0 and kt_α, the average of $Di_{t_0}^{\propto}$ across RF_i's is obtained for a given α with its reciprocal later computed [Eq. (18)]. This produces a known range of the magnitude for $\vec{f_C}$ and $\vec{f_P}$ and with this k_0, and kt_α is selected to ensure $\vec{f_T}$ and $\vec{f_S}$ are in the same order of magnitude as $\vec{f_C}$ and $\vec{f_P}$:

$$\vec{f_C} = kc_\alpha \vec{U}_{rm_C} rm_C r_1^\alpha, \tag{14}$$

$$\vec{f_P} = kp_\alpha \vec{U}_{rm_P} rm_P r_2^\alpha, \tag{15}$$

$$\vec{f_T} = kt_\alpha \vec{U}_{rm_T} rm_T |s|, \tag{16}$$

$$\vec{f_S} = k_0 r_0, \tag{17}$$

$$k_\alpha = \frac{1}{\left(D_i^\alpha\right)}, \tag{18}$$

$$\vec{f_R} = \vec{f_C} + \vec{f_P} + \vec{f_T} + \vec{f_S}. \tag{19}$$

III. RESULTS

A. Simulations

Most of the previous functional and neurophysiological studies that have explored the spatiotemporal dynamics that could characterize P_{RE} were conducted using foveated biological systems. This has two very important consequences. One, the simulation results we will use here to systematically assess the phenomenological validity of the proposed model are limited to the extant literature. Two, as all rigorous models should strive toward, reported simulations will provide a rich

and clear set of predictions that should inform future investigations of P_{RE}, especially those that are conducted using afoveated systems.

In the subsequent sections, despite proposing the underlying causes of P_{RE}, modular components included in the model as well as their interactions within specific temporal windows were independently and rigorously explored. We opted for this approach to avoid the theoretical demands of the proposed model as well as experimental demands from previous studies. In addition to this, the principal parameter α was systemically explored as well as the extent foveated systems require the presence of elφ's to implement P_{RE}. Specifically, for the simulation results reported below, the underlying architecture consists of two main layers: a retinotopic field and a force field. The retinotopic field is composed of hexagonal overlapping RF_i's that tile the foveal, parafoveal, and peripheral extent of visual space, with more RF_i's tiling the foveal extent. Each RF_i possessed corresponding eccentricity-dependent elφ's. Force fields perturb RF_i's from their equilibrium positions. This field is activated by the availability of attentional-oculomotor signals which align with early visually transient signals, the selection of a peripheral site, and later retinotopically modulated transient signals [15,22]. The perturbation of RF_i's produces spatiotemporal retinotopic trajectories which manifest in time-varying modulation of density at a given retinotopic location of visual space.

We modeled each RF_i as a bivariate Gaussian kernel function G, Eq. (20). To then obtain a probability density estimate for a single retinotopic location, perturbed by a neuronal force field, Eq. (21) was implemented. Each retinotopic location is represented by two vectors $rl_1 = [rl_{11}, rl_{12}, rl_{13}, \ldots, rl_{1n}]$ and $rl_2 = [rl_{21}, rl_{22}, rl_{23}, \ldots, rl_{2n}]$, where $rl_i = (rl_{1i}, rl_{2i})$ denotes the retinotopic location whose population neural density (or sensitivity) is sampled from the bivariate distribution $\hat{D}$. Here, B denotes the bandwidth used, with G_B as a non-negative and symmetric function ($\int G_B(u)du = 1$) defined in bivariate terms as $B^{-1/2}\, G(B^{-1/2_u})$:

$$G(u) = \frac{1}{\sqrt{2\tau}} \exp\left(\frac{1}{2}\, u^t u\right), \tag{20}$$

$$\hat{D}(rl,\ \mathbf{B}) = \frac{1}{n} \sum_{i=1}^{n} G_{\mathbf{B}}(rl - rl_i). \tag{21}$$

Population density levels at the following retinotopic locations along the path of the impending saccadic eye movement (i.e., the radial axis) were sampled: outer foveal ($rad_{fov\text{-}out}$), inner foveal/inner parafoveal ($rad_{fov+para\text{-}in}$), outer parafoveal/inner peripheral ($rad_{para+peri\text{-}in}$), and outer peripheral ($rad_{peri\text{-}out}$) for a given simulation. Specifically, the $rad_{fov+para\text{-}in}$ and $rad_{para+peri\text{-}in}$ locations are points distributed across visual space (foveal, parafoveal, and peripheral extent) that connects the fovea to the saccade target, while the $rad_{fov\text{-}out}$ and $rad_{peri\text{-}out}$ locations are points that also lie along the radial axis but fall outside of the foveal-target extent (Fig. 5).

It is important to highlight two very important points as it pertains to simulations at these retinotopic locations. One, results reported below are from when the centripetal force is fully turned on (const., $t_{x2} < t < t_{x3}$) to when all forces including the centripetal force are turned off. The selection of this temporal window is consistent with previous remapping studies in foveated systems, where the organism is instructed to first acquire fixation and only after maintaining fixation allowed to preselect the peripheral target and then later execute a saccadic eye movement in the corresponding direction. Finally, because neural sensitivity is lower at the more eccentric locations in visual space than the more central locations during fixation (at t_0), we controlled for known eccentricity effect [75] by dividing the estimated raw population density readouts (which are analogous to raw population neural sensitivity) at each sampled location with the mean of the first 110 ms (i.e., the temporal window $\vec{f_C}$ is in a steady state).

1. Centripetal component

When modeled RF_i's constrained by their elφ's were perturbed by only a centripetal force [Figs. 5(a) and 5(b)], we found distinguishable differences in population density levels between more foveal ($rad_{fov\text{-}out}$ and $rad_{fov\text{-}in}$) and more eccentric ($rad_{para+peri\text{-}in}$ and $rad_{peri\text{-}out}$) locations during the sustained period of this force. Within a postsaccadic window, the decline of the centripetal force was accompanied by a clear handoff in population density levels between the foveal and peripheral locations. We found an earlier and stronger increase in population density levels at the outer peripheral location ($rad_{peri\text{-}out}$), followed by an increase in density levels at the inner peripheral location ($rad_{para+peri\text{-}in}$). These results suggest that foveal retinotopic locations enjoy a disproportionate amount of the resources of the visual system just before the onset of a saccade [62]. It is thus likely that these resources, which result in high levels of neural sensitivity and directly support sustained and/or high levels of visual sensitivity at the foveal region of visual space [63], are predictively reallocated toward the peripheral region so that there is an appropriate level of postsaccadic sensitivity at the selected target extent just before the eye lands in the periphery [36].

2. Convergent component

Under the perturbation by a convergent force alone [Figs. 5(c) and 5(d)], within a midpresaccadic window, we found a graded decline in population density levels across visual space. Under a strong inverse force field, the onset of a convergent force causes RF_i's that support outer parafoveal and outer peripheral locations ($rad_{para+peri\text{-}in}$ and $rad_{peri\text{-}out}$) to allocate their density toward the saccade target, while at the foveal and inner parafoveal locations ($rad_{fov\text{-}out}$ and $rad_{fov\text{-}in}$), density levels remain largely stable. These results suggest that convergent signals are limited and do not provide presaccadic sensitivity advantages around a preselected peripheral site. On one level, this result is deeply counterintuitive, as one might expect convergent signals to produce effects that align with the convergent form of remapping. On another level, this finding is consistent with a more recent functional study [28] and a growing number of neural studies which suggest that the functional and neural correlates of the convergent form of P_{RE} fundamentally require an additional component [21,22].

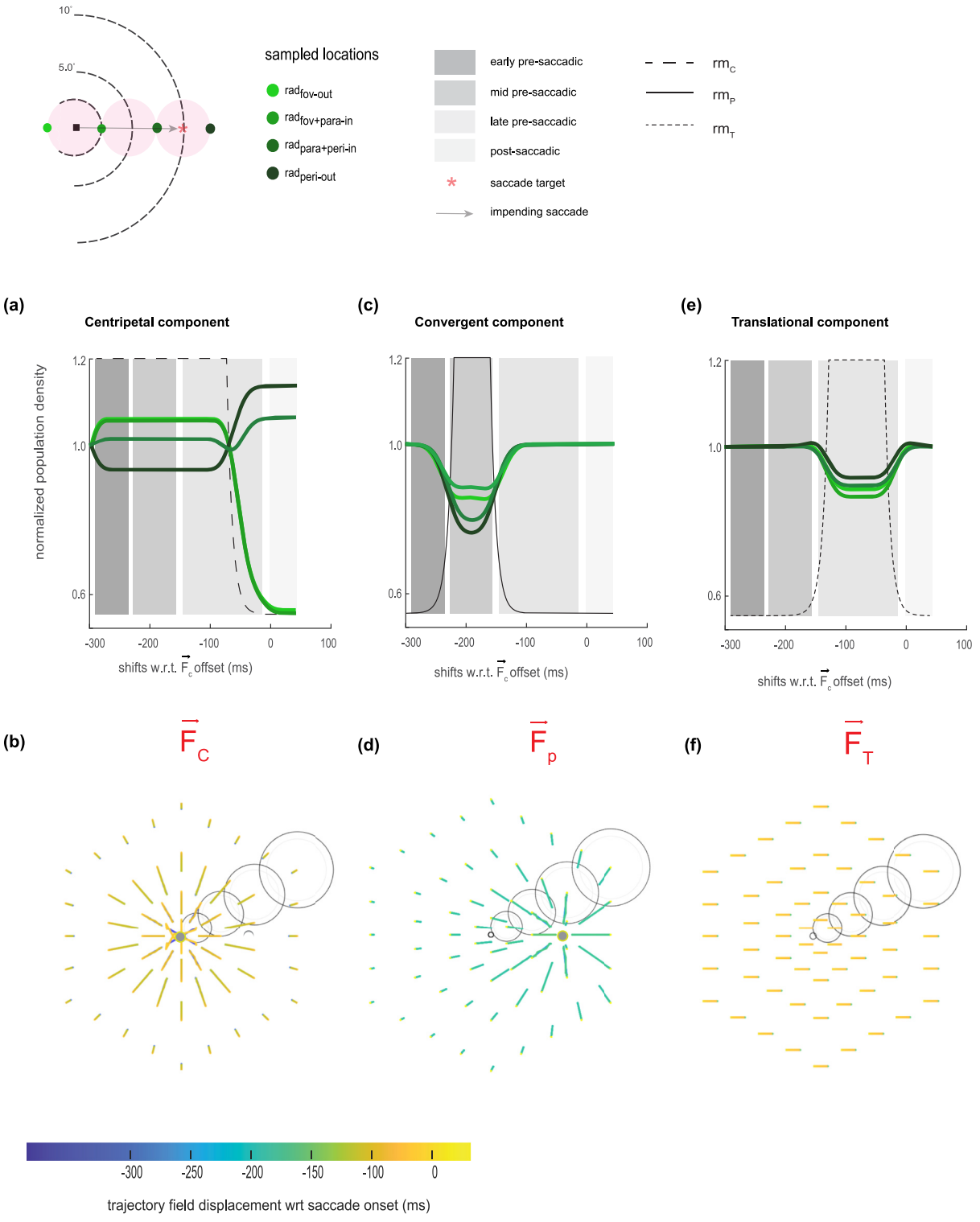

FIG. 5. Single force simulations under an inverse force field. Simulation results (a), (c), and (e) at $\alpha = -1.6$ in cases when RF_i's are perturbed by a single external force constrained by elφ's. Along the x axis represents the simulation time sampled at discrete increments of 1 ms realigned with respect to the offset of the central force (i.e., modeled as the saccade onset). (b), (d), and (f) are corresponding spatiotemporal trajectories used to compute population density readouts.

3. Translational component

Like the simulations for the purely convergent case, we found a graded decline in population density levels across visual space due to a pure translational force applied during a late presaccadic window [Figs. 5(e) and 5(f)]. However, here, changes in population density levels favor the future center of gaze over the current center of gaze. These results align with the predictions proposed by early neurophysiological studies that the anticipatory transferring of neural sensitivity from

the current field of a cell to its future postsaccadic location is in part driven by oculomotor modulated translational signals [16–19,68,71]. Behaviorally speaking, this transferring of neural sensitivity results in a relatively equal and transient decline in visual sensitivity across visual space [76].

4. Centripetal and convergent components

The combination of centripetal and convergent forces [Figs. 6(a) and 6(b)] resulted in an amplification of the differences in population density levels along the radial axis during the application of the convergent force [compare with individual force simulations in Fig. 6(b)], while preserving the handoff noted earlier for the centripetal only simulation. Together with the centripetal simulation, these results predict the importance of the centripetal force in not only maintaining the appropriate level of neural sensitivity at the current center of gaze during the sustained period of the force (i.e., at the time of fixation) but also ensuring the immediate availability of postsaccadic visual sensitivity at the future center of gaze during the offset of the force [Figs. 5(a) and 6(a)].

5. Centripetal and translational components

The combination of the centripetal and translational forces resulted in an amplification of the divergence in density between the foveal and peripheral locations during the application of the translational force, while retaining the foveal-peripheral handoff during the decline of the centripetal force [Figs. 6(c) and 6(d)].

6. Convergent and translational components

With the combination of a convergent force and an increasing influence of a translational force, we found moderate asymmetric increases in population density levels at the $\text{rad}_{\text{para+peri-in}}$ and $\text{rad}_{\text{peri-out}}$ locations [Figs. 6(e) and 6(f)] when compared with the simulation by a convergent force alone [Figs. 5(c) and 5(d)]. No other simulation produced these changes in density levels in the periphery. On the neural domain, these transient increases in population density levels are consistent with a previous study that has shown transient increases in neural sensitivity in the frontal eye fields [21], which most likely corresponds to the preselection of the saccade target (i.e., a precursor of convergent remapping or the dynamics that initiates P_{RE} in general). On the behavioral domain, these results align with the prediction that increases in visual sensitivity just before saccade onset at a preselected peripheral site are not always symmetric [20,59–61].

7. All components

The single and paired force simulations indeed capture specific components from the extant literature. These simulations, however, failed to conform to the idea that convergent signals alone or convergent along with translational signals provide significant neural sensitivity advantages around the preselected peripheral site when compared with more distal locations (i.e., extents that are further away from the saccade target). This begs the question: does the combination of a centripetal, convergent, and translational force lead to such advantages? To directly investigate this question, we next conducted a simulation that included all three forces. To foreshadow these results, despite measurements from previous studies being tied to a specific retinotopic brain structure, the sampling of different retinotopic locations, and differences in quantification methods, results simulated by the proposed model revealed spatiotemporal dynamics that succinctly captured the essence of two very important empirical observations frequently cited in support of the translational [18] and convergent [22] forms of P_{RE} (see Fig. S1 in the Supplemental Material [77]).

Specifically, within an early presaccadic window, we found a graded profile of neural density along the radial axis [55]: an immediate and sharp decline at the outer peripheral region ($\text{rad}_{\text{peri-out}}$), a modest decline at the outer parafoveal region ($\text{rad}_{\text{para+peri-in}}$) [Fig. 7(a)], and sustained levels of neural density in the foveal ($\text{rad}_{\text{fov-out}}$) and inner parafoveal ($\text{rad}_{\text{fov+para-in}}$) regions [Fig. 7(a)]. This was followed by a modest rebound in density readout within a midpresaccadic window at the more eccentric locations ($\text{rad}_{\text{peri-out}}$ and $\text{rad}_{\text{para+peri-in}}$) from 240 to 130 ms before saccade onset, consistent with the prediction of the model related to the role of pure convergent signals. Within a late presaccadic window just before saccade onset, we found continued declines in density levels at locations near the current center of gaze ($\text{rad}_{\text{fov-out}}$, $\text{rad}_{\text{fov+para-in}}$). Within this same temporal window, we found a clear jump in neural density levels at a future postsaccadic location ($\text{rad}_{\text{peri-out}}$) when compared with the more parafoveal extent ($\text{rad}_{\text{para+peri-in}}$). These results qualitatively match the neural sensitivity signatures reported by Sommer and Wurtz [18]. As their results also predict, this jump in density followed a growing difference in density levels between the $\text{rad}_{\text{peri-out}}$ location when compared with the more parafoveal location as the simulation approached saccade onset [Figs. 7(a) and 7(b)].

Finally, within a later presaccadic window along with an overlapping postsaccadic window, we found declines in postsaccadic density levels at locations furthest away from the saccade target ($\text{rad}_{\text{fov-out}}$, $\text{rad}_{\text{fov+para-in}}$), while the location close to the saccade target ($\text{rad}_{\text{para+peri-in}}$) and an even closer extent ($\text{rad}_{\text{peri-out}}$; i.e., spatial extents around the simulated saccade target) demonstrated clear neural density advantages. Remarkably, these dynamics, which temporally align with the canonical order of presaccadic events [15], qualitatively match results reported by Hartmann *et al.* [22] [Fig. 8(b)]. These results reveal the importance of a declining centripetal force in implementing the convergent form of P_{RE}, while the declining translational signals can further amplify visual sensitivity around a preselected peripheral site. Taken together, the recapitulation of the results by Sommer and Wurtz [18] and Hartmann *et al.* [22] provides the long sought-after computational evidence that P_{RE} is fundamentally a dynamic phenomenon which includes centripetal, convergent, and translational components [24–27].

Additionally, the three-force simulation can explain conflicting neural findings related to whether P_{RE} is limited to the current and future postsaccadic locations. Specifically, classical neurophysiological studies have shown that RF_i's respond to a salient cue placed within their future RF before the onset of an eye movement [16–19]. However, more recent results by Wang *et al.* [55] suggest that cells in lateral intrapari-

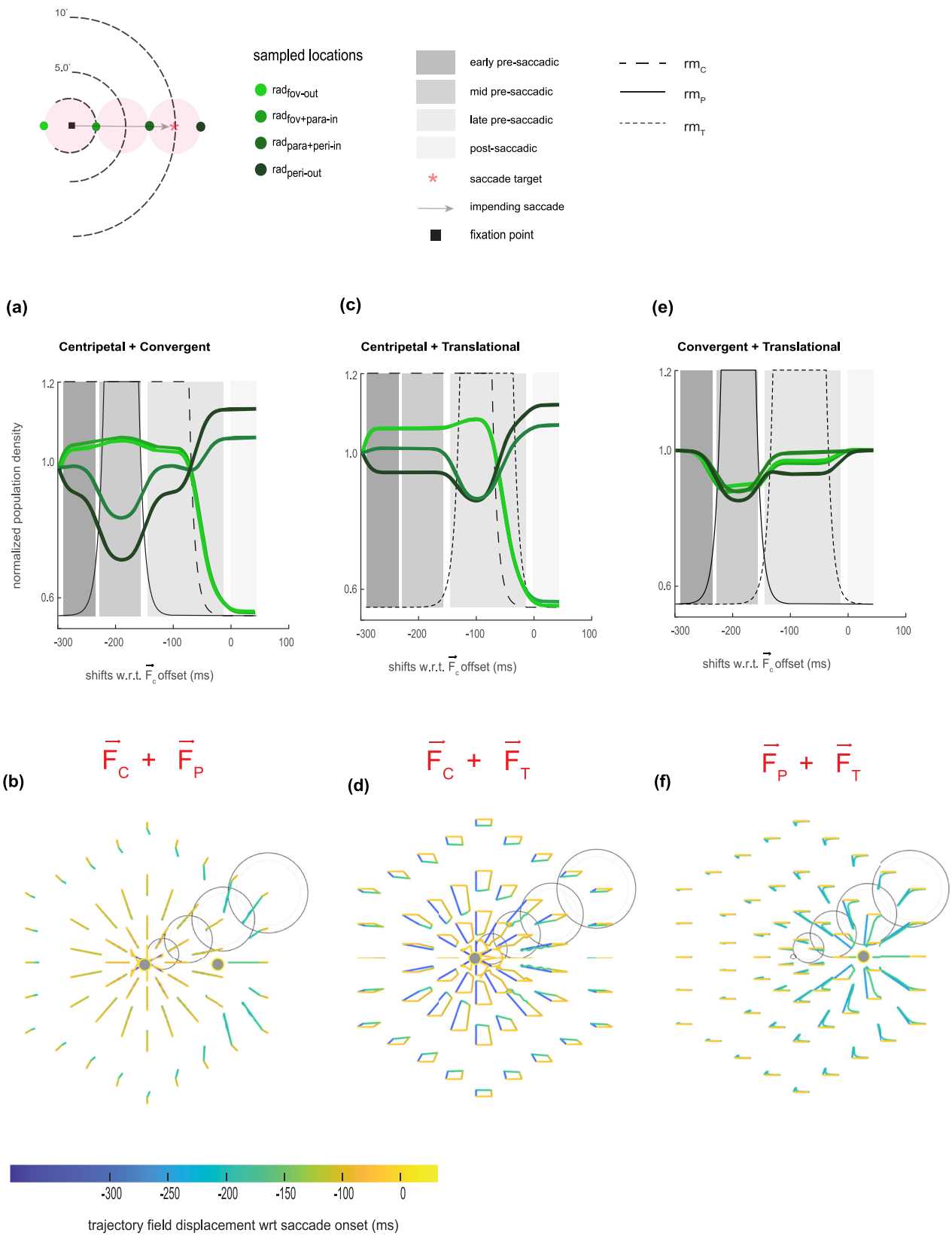

FIG. 6. Two force simulations under an inverse force field. Simulation results (a), (c), and (e) at $\alpha = -1.6$ in cases when RF_i's are perturbed by two external forces constrained by eccentricity-dependent elφ's. (b), (d), and (f) are corresponding spatiotemporal trajectories.

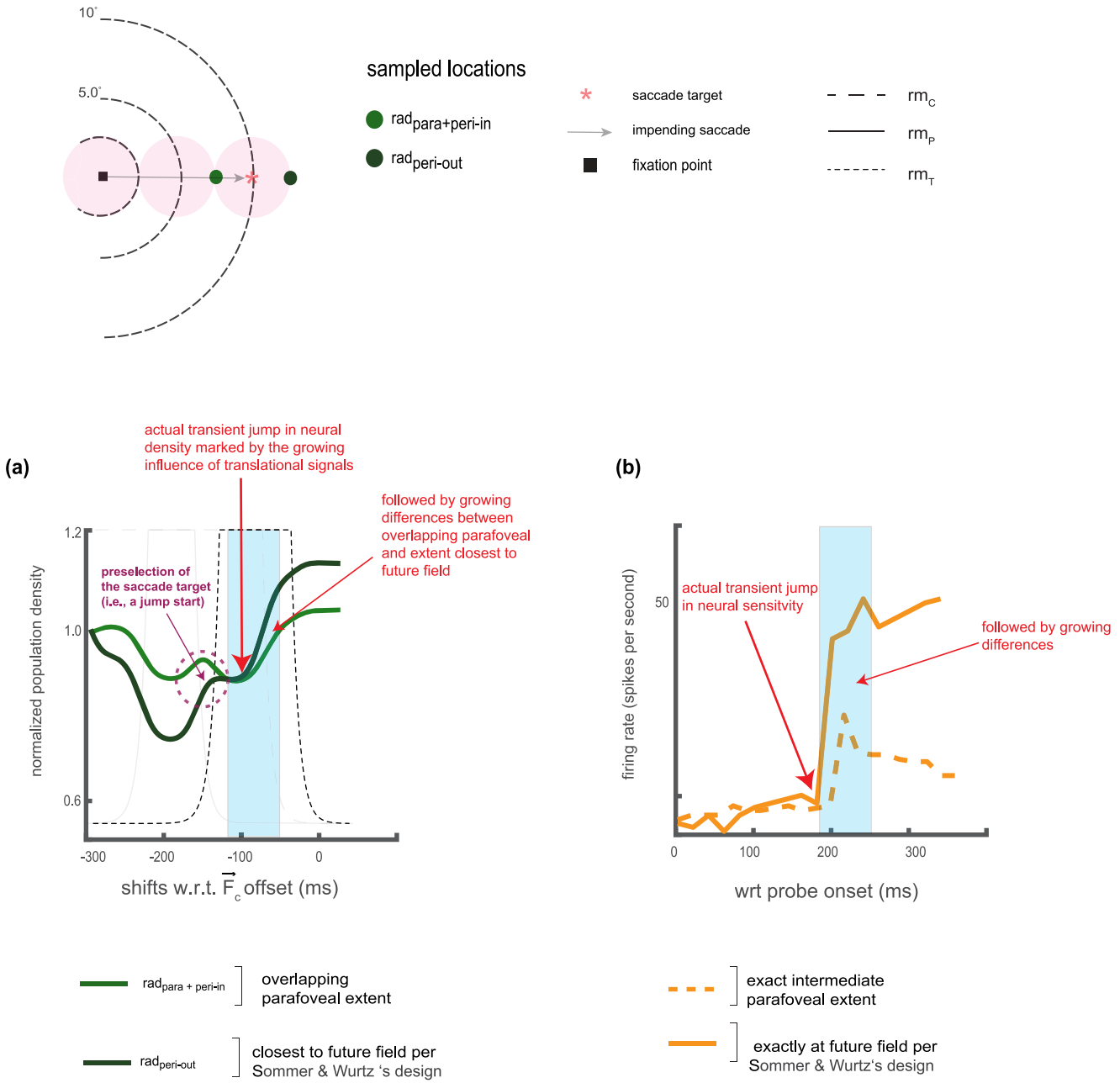

FIG. 7. The combination of a centripetal, convergent, and translational signals under an inverse force field qualitatively recapitulates translational effects reported by Sommer and Wurtz [18]. (a) Simulated population signatures constrained by eccentricity-dependent elφ's, under distinct inverse force fields of varying strengths. Along the x axis represents the simulation time sampled at discrete increments of 1 ms. (b) Cartoon of results reported by Sommer and Wurtz [18]. See Fig. 2(c), right panel, for exact plots.

etal cortex also become responsive to intermediate locations along the saccade trajectory. This is said to drive activity in favor of the current center of gaze that is eventually redirected (or remapped) toward the future postsaccadic location of the cell. The three-force simulation strongly suggests that graded changes in sensitivity toward the fovea occur uniquely within an early to midpresaccadic window (e.g., during early trainset signals), as predicted by Wang *et al.* [55]. However, these graded changes in sensitivity cease within a late midsaccadic and late presaccadic window just before saccade onset.

8. Exploring different α values

To assess the impact of the spatial profile of the force fields, we repeated the three-force simulations with different values of α, Figs. 9(a) and 9(b). With $\alpha = -1$ (i.e., a moderate inverse force field), population density signatures at the more foveal locations are largely unchanged when compared with simulated results under a strong inverse force field where α is set to -1.6. More eccentric RF_i's are sensitized toward the current center of gaze but less so when compared with a strong inverse force field. To this end, within an early midpresaccadic window, we found declines in population density levels at

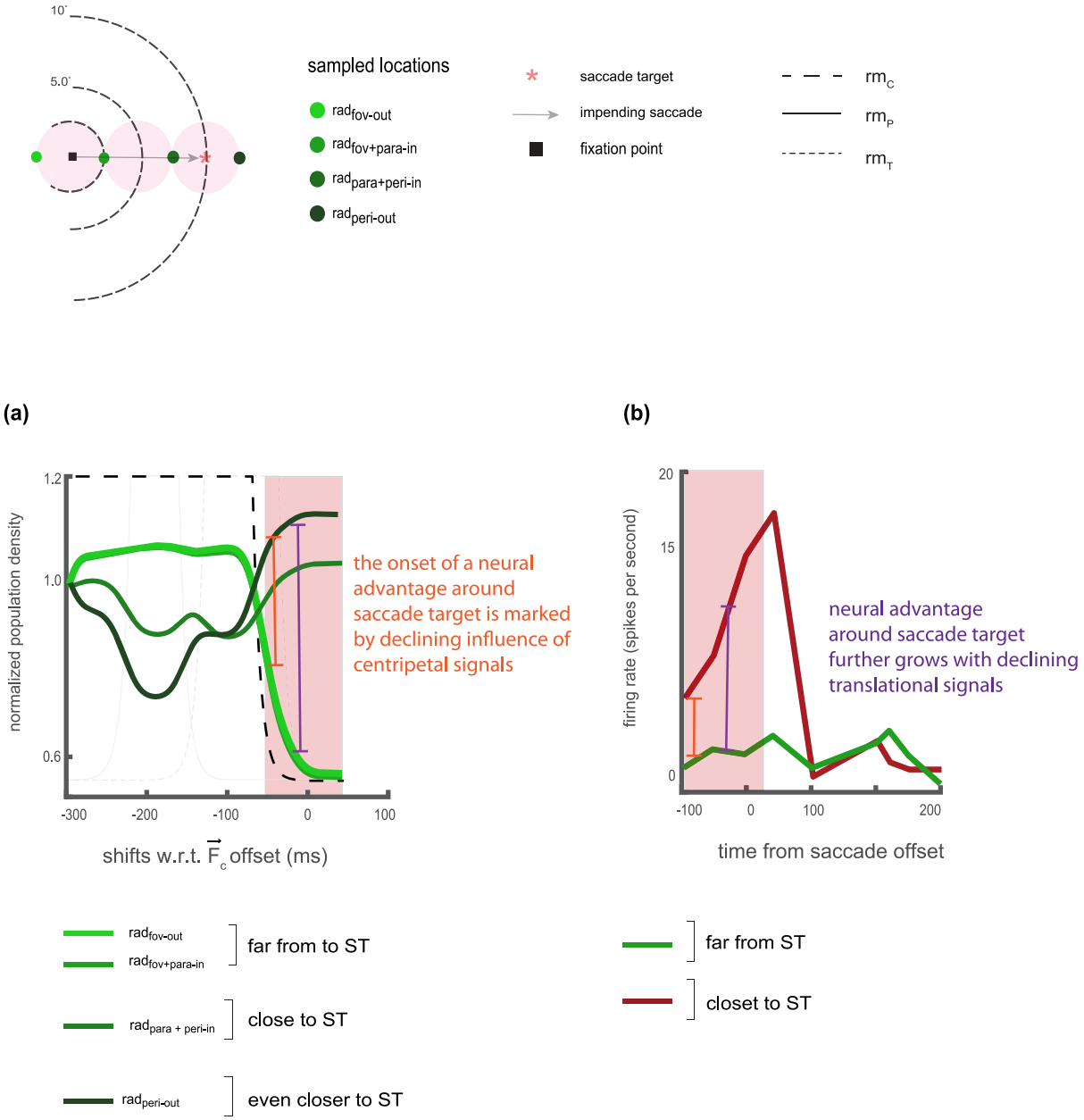

FIG. 8. The combination of a centripetal, convergent, and translational signals under an inverse force field recapitulates convergent effects reported by Hartmann *et al.* [22]. (a) Simulated population signatures constrained by eccentricity-dependent elφ's under an inverse force field. Along the x axis represents the simulation time sampled at discrete increments of 1 ms. (b) Cartoon version of results reported by Hartmann *et al.* [22]. See Fig. 1(b) for the exact plot.

the $\text{rad}_{\text{para+peri-in}}$ and $\text{rad}_{\text{peri-out}}$ locations. However, declines at the $\text{rad}_{\text{peri-out}}$ location were not as large when compared with what we observed under a stronger inverse force field. Under a weak inverse force, where α is set to -0.6, intermediate parafoveal RF_i's are more sensitized toward the current of gaze. To this end, we observed larger declines in population density levels at the $\text{rad}_{\text{para+peri-in}}$ location than the simulations under a strong inverse force field. Biological systems are stochastic and sloppy, physical systems less so [78–81]. It is thus a certainty that, between and within different biological systems, within different visual and movement contexts, α will vary. However, considering that stimulations under a moderate force field, as opposed to a weaker one in part, resemble signatures under a strong inverse force field, these results strongly suggest, at least in foveated systems, that P_{RE} likely obeys an inverse distance law (e.g., $P_{RE} \propto \frac{1}{r^{1.6}}$).

9. *Exploring the architectural space*

The results we have presented thus far were simulated with modeled RF_i's constrained by eccentricity-dependent elφ's. To directly assess the role of elφ's on presaccadic and postsaccadic density readouts, we ran two additional simulations (both under a strong inverse force field, $\alpha = -1.6$). For the first stimulation, $\rho\beta$ was assumed with c set to a scalar >1, while in the second stimulation, $\rho\alpha$ was assumed with c set

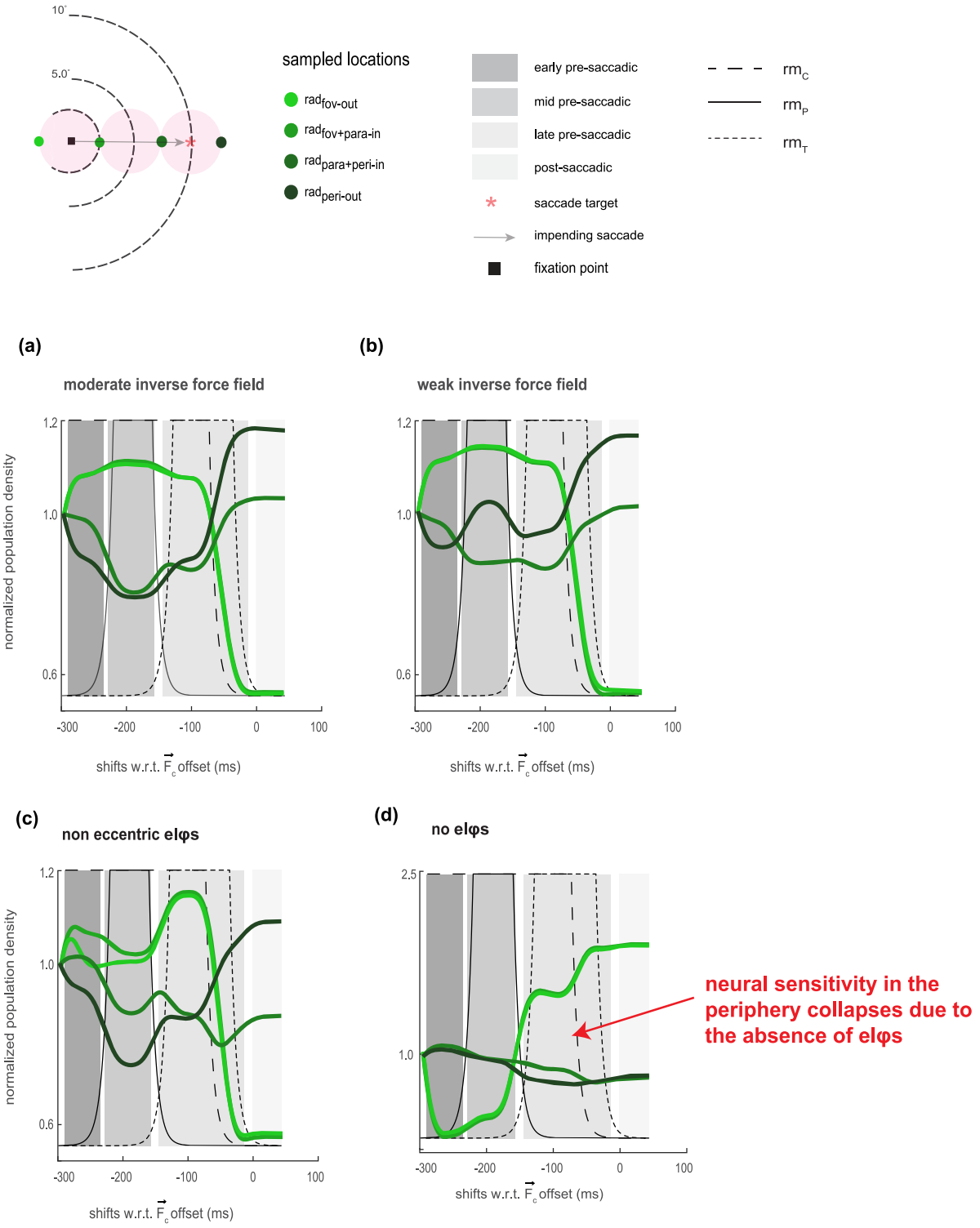

FIG. 9. Additional three force simulations under an inverse force field. Simulated population density constrained by eccentricity-dependent elφ's, under distinct inverse force fields of varying strengths: (a) $\alpha = -1.0$ and (b) $\alpha = -0.6$. Simulated population density for the combination of three independent forces that are (c) constrained by noneccentricity-dependent elφ's or (d) unconstrained.

to 0. In the case of an eccentricity-independent tilling of elφ's, we found no appreciable differences in density levels when compared with the signatures we observed under eccentricity-dependent constraints during the early midpre-saccadic periods [Fig. 9(c), compare with Figs. 7 and 8]. However, a different signature emerges with the introduction of a translational force. Specifically, we found that sustained density levels at the foveal regions increase in magnitude, while there is a marked decrease in density level at the more intermediate eccentric location. Eccentricity-dependent elφ's allow more eccentric RF_i's a greater movement extent (i.e., more elasticity). Under a noneccentricity-dependent configu-

ration, however, eccentric RF_i's are much more restricted in their ability to shift within the visual field. Consequently, once eccentric RF_i's become sensitized toward the current center of gaze, they become restricted from reallocating these resources back toward the periphery. This results in an inappropriate level of sensitivity at the current center of gaze within a late presaccadic window as opposed to locations around the future center of gaze. Finally, for simulations where RF_i's were unconstrained by their elφ's, retinotopic organization simply collapses [Fig. 9(d)]. The centripetal force results in an overcompression toward the current center of gaze, with the peripheral region experiencing radical declines in sensitivity. Further, despite the onset of the convergent force (e.g., the looming presence of a predator, nearby car), RF_i's are largely desensitized to the presence of these forces [82–84]. This result points to the importance of elφ's in preventing any radical and unsustainable forms of remapping while ensuring that retinotopic organization is always maintained.

B. Psychophysics

To now assess the biological plausibility of the model and its predictive power directly, we conducted three psychophysics experiments in foveated systems (human subjects). Specifically, we assessed changes in visual sensitivity which we posit is supported by population neural density (or sensitivity), across visual space using a cued saccade task (Fig. 10). To do this, we carefully mapped the geometry of visual space with the intent to examine transient consequences of predictive remapping on visual sensitivity changes at precise points along the saccade trajectory (radial axis), matching the locations we simulated using the proposed model. In addition, symmetric points orthogonal to the saccade trajectory (tangential axis) were measured. Visual sensitivity measurements were obtained while human subjects fixated, selected a target on the peripheral retina, planned, and executed a saccadic eye movement toward the peripheral target. Specifically, radial points at foveal ($\text{rad}_{\text{fov-out}}$, $\text{rad}_{\text{fov-in}}$), parafoveal ($\text{rad}_{\text{para-in}}$, $\text{rad}_{\text{para-out}}$), and peripheral ($\text{rad}_{\text{peri-in}}$, $\text{rad}_{\text{peri-out}}$) locations, and tangential points symmetric to one another with respect to the radial axis at foveal ($\text{tan}_{\text{fov-ccw}}$, $\text{tan}_{\text{fov-cw}}$), parafoveal ($\text{tan}_{\text{para-ccw}}$, $\text{tan}_{\text{para-cw}}$), and peripheral ($\text{tan}_{\text{peri-ccw}}$, $\text{tan}_{\text{peri-cw}}$) locations were probed before and after the central movement cue [Fig. 10(a)].

In each trial, a low-contrast probe was flashed at one of these locations (chosen at random) for 20 ms with 75% probability; in 25% of trials (control trials), no probe was flashed. The contrast of the probe stimuli was chosen (independently for each subject and for each spatial location cluster; see Methods in the Supplemental Material [77]) such that the detection probability was at 50% in the absence of eye movements. The probes were presented at a random time from 600 ms before to 360 ms after the central movement cue. This experimental paradigm was attractable for two reasons. One, most remapping studies typically sample locations in space favorable to one form of remapping over another. However, with this dense spatial sampling of visual space, this allowed us to assess the possible primary role the centripetal, convergent, and translational components at play in modulating visual sensitivity within distinct regions of visual space. Finally, measuring visual sensitivity along and around the entire saccade trajectory, within early presaccadic (−300 to −250 ms with respect to saccade onset), midpresaccadic (−250 to −150 ms), late presaccadic (−150 to −5 ms), and postsaccadic (−5 to +150 ms) windows was critical in assessing the consequences of P_{RE} on visual sensitivity within a larger presaccadic and postsaccadic window [Fig. 10(b)].

Subjects reported whether they were able to detect the flashed probe using a push button. The control (no probe) trials allowed us to assess the incidences of false alarms. Low false alarm rates of 1.2, 1.4, and 1% (along the radial, tangential counterclockwise, and clockwise axes, respectively) gave me high confidence about the visual sensitivity reports of the subjects. we collected ∼21 000 trials, with a minimum of 1500 trials per subject. Control trials were excluded from the main analyses. We calculated the normalized average visual sensitivity of 11 subjects as a function of flashed probe times relative to saccade onset (see Fig. S2 in the Supplemental Material [77] for control readouts between groups for the parafoveal and peripheral experiments). Corresponding error estimates were obtained using a 20-fold jackknife procedure in which the sensitivity was estimated from 95% of the data (see Methods in the Supplemental Material [77] for experimental protocol and details regarding behavioral analyses).

Within an early presaccadic window (−300 to −250 ms), a graded visual sensitivity profile along the radial axis was observed, consistent with changes in neural sensitivity levels reported by Wang *et al.* [55] and simulated results [Figs. 8, 9, and 11(a), left panel]. Within a midpresaccadic window (−250 to −150 ms) before saccade onset, a modest rebound (or a jumpstart) in visual sensitivity at the $\text{rad}_{\text{peri-out}}$ and $\text{rad}_{\text{para+peri-in}}$ locations was observed, consistent with the predicted role of convergent signals and simulated results. Continued declines in visual sensitivity at locations near $\text{rad}_{\text{fov-out}}$, $\text{rad}_{\text{fov+para-in}}$ were observed and consistent with changes in neural sensitivity reported in classical neurophysiological findings [16–19] as well as simulation results. Declines in sensitivity at the $\text{rad}_{\text{fov-out}}$, $\text{rad}_{\text{fov+para-in}}$ location were observed along with a jump in late presaccadic (−150 to −5 ms) sensitivity at the $\text{rad}_{\text{peri-out}}$ location. Finally, within a postsaccadic window, continual declines in postsaccadic sensitivity at the $\text{rad}_{\text{fov-out}}$, $\text{rad}_{\text{fov-in}}$ location were observed along with a sharp and immediate increase in postsaccadic (−5 to +150 ms) sensitivity at the $\text{rad}_{\text{peri-out}}$, $\text{rad}_{\text{para+peri-in}}$ locations.

Observations of visual sensitivity changes along the tangential axes largely mirrored those along the radial axis in an eccentricity-dependent fashion [Fig. 11(a), right panel]. We found a decrease in sensitivity at the $\text{tan}_{\text{peri-ccw+cw}}$ location within the early presaccadic window. This was accompanied by a modest increase in midpresaccadic sensitivity in the parafoveal region ($\text{tan}_{\text{para-ccw+cw}}$) or sustained levels of sensitivity in the foveal ($\text{tan}_{\text{fov-ccw+cw}}$) region. Like the radial axis, we observed a rebound in late presaccadic sensitivity (−50 ms from saccade onset) at the most eccentric location ($\text{tan}_{\text{peri-ccw+cw}}$) that was followed later and less marked rebound at the parafoveal location ($\text{tan}_{\text{para-ccw+cw}}$). A continued decline in postsaccadic sensitivity at the foveal location was accompanied by rapid increases first at the peripheral locations followed by the parafoveal location.

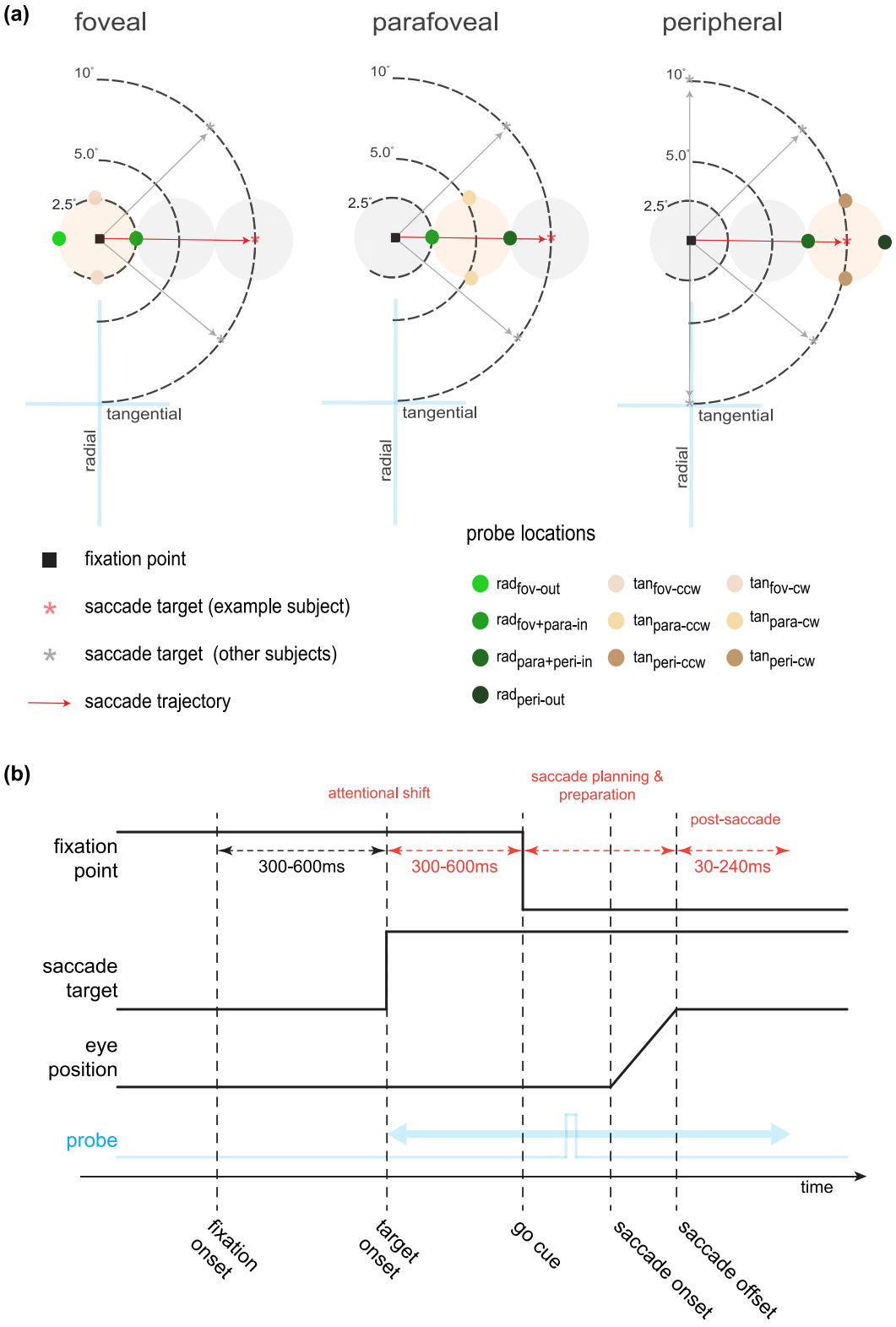

FIG. 10. Cued probe-detection task. (a) Spatial locations tested across experiments. Colored circles show the locations at which a low-contrast probe was flashed as subjects planned and prepared a saccade (black arrow) toward the periphery. Probe locations are shown only for horizontal saccades to the right. For other saccade target locations, the probe locations were appropriately positioned along and around the path of a saccade. In the foveal and parafoveal experiments, a saccade target (gray or red asterisk) was presented at azimuth angles of 0°, 45°, and 315° (each subject had a different angle). In the peripheral experiment, the saccade target was presented either at azimuth angles of 0°, 45°, 90°, 270°, or 315° (each subject had a different angle). (b) Temporal sequence of an example trial. The start of a trial began with the appearance of a fixation point, followed by a time-varying presentation of the saccade target. A low-contrast probe was flashed either before the onset of the central movement cue (the presaccadic condition) or after (the postsaccadic condition).

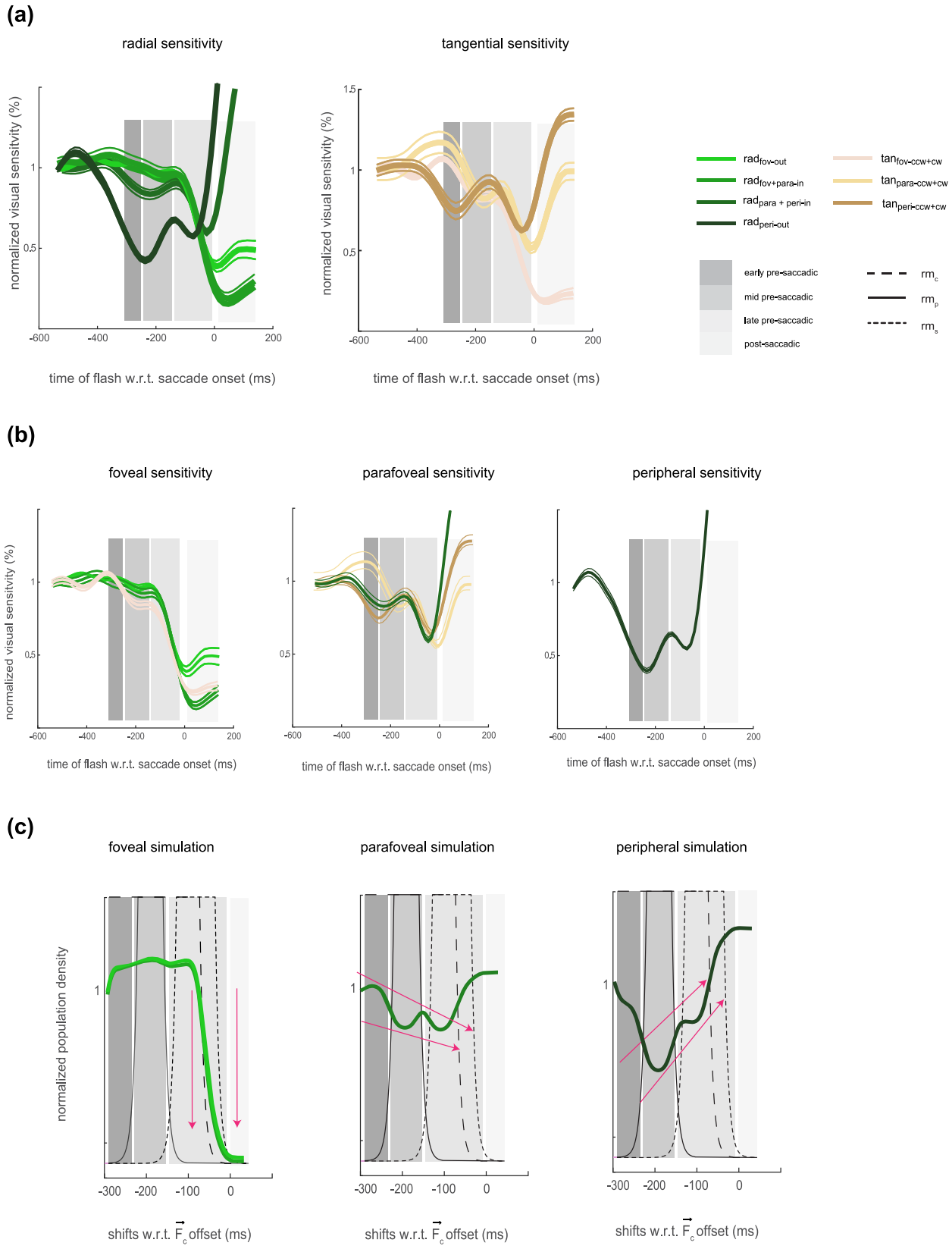

FIG. 11. Sensitivity functions across visual space within distinct presaccadic and postsaccadic windows. (a) Thick solid lines represent normalized changes in presaccadic and postsaccadic sensitivity as a function of flashed probe times relative to saccade onset along and around the saccade trajectory ($n = 11$). The thin lines represent corresponding error estimates obtained using a 20-fold jackknife procedure in which the sensitivity was estimated from 95% of the data. (b) Presaccadic and postsaccadic sensitivity and (c) simulation results grouped within the different regions of visual space.

Quite convincingly, the combination of three independent forces largely predicts visual sensitivity readouts along the radial and tangential axes, except for the $\tan_{\text{peri-ccw}}$ location during an early and midpresaccadic window. This is particularly clear when both the experimental and simulated data are grouped into the foveal, parafoveal, and peripheral groups [Figs. 11(b) and 11(c)]. Furthermore, these results point to the biological plausibility and generalizability of the proposed model. On one level, these results contradict a set of functional studies that support the translational form of P_{RE} [30,31], all of which suggest that there is no spreading of neural resources around the preselected saccade target. On another level, the principal suggestion from these functional studies holds that pure convergent signals cannot provide the type of neural advantages around the saccade target that previous neural studies have reported [Figs. 5(c) and 5(d)]. To conclude, increases in postsaccadic sensitivity, which we posit is supported by increase in population neural sensitivity, at the locations around the saccade target ($\tan_{\text{peri-ccw+cw}}$, $\text{rad}_{\text{peri-out}}$, $\text{rad}_{\text{para+peri-in}}$) compared with the more distal locations ($\tan_{\text{fov-ccw+cw}}$, $\text{rad}_{\text{fov-out}}$, $\text{rad}_{\text{fov+para-in}}$) provide the long sought-after functional evidence in support of the convergent form of P_{RE}. It is thus likely that the allocation of these neural advantages toward the saccade target is primarily the result of a declining centripetal signals with translational signals playing more of a secondary role.

C. Rhythmicity

Having demonstrated that P_{RE} is a dynamic phenomenon that includes the newly discovered centripetal component along with convergent and translational components, we next wanted to assess a core assumption of the model, that is, early visually transient and feedback transient signals are uniquely supported by delta rhythmicity (2–4 Hz), which happens to align with the rate foveated systems make saccadic sys movement [34]. Indeed, this rhythmic band is known to predict attentional shifts before the onset of a saccadic eye movement [67].

We hypothesized that attentional signals are highly selective toward the current and future center of gaze, while at intermediate parafoveal locations, retinal image displacement signals blunt attentional resources that would otherwise persist at these locations. To test this, we assessed the spectral signature underlying the observed changes in sensitivity [85]. The logic behind this assessment is as follows: If these changes in the center of gaze and the peripheral region where the saccade target resides are a consequence of attentional shifts, then the spectral signature associated with changes in sensitivity at these locations should be statistically significant and resemble if not match known rhythmic patterns of attentional shifts during fixation and the selection of the peripheral target. Conversely, in the parafoveal region, observed rhythmic patterns should not be associated with attentional shifts. To this end, if the spectral architecture we find fails to recapitulate these known rhythmic patterns in the foveal and peripheral regions or are statistically significant in the parafoveal regions, then sensitivity changes at the center of gaze and peripheral region cannot be directly attributed to attentional shifts.

Transforming detrended time series sensitivity data (Fig. S3 in the Supplemental Material [77]) into the frequency domain, we found that visual sensitivity around the current center of gaze (foveal) locations ($\text{rad}_{\text{fov-out}}$, $\text{rad}_{\text{fov+para-in}}$) exhibited rhythmicity within a delta spectral window at ∼2 Hz, except for the $\tan_{\text{fov-ccw+cw}}$ location which exhibited rhythmicity that bordered the delta and theta windows at ∼3 Hz [Fig. 12(a)]. Spectral differences calculated using location shuffled data ($n = 1500$) vs the nonshuffled data at these locations were statistically significant (two-tailed paired-sample t test, $P = 0.0018$, 0.0236, and 0.0018). These results are consistent with the idea that delta rhythms at ∼3 Hz actively mediate presaccadic attentional shifts at suprathreshold levels [67,86–88]. At the intermediate (parafoveal) locations ($\tan_{\text{para-ccw+cw}}$), we found that sensitivity exhibited delta-band rhythmicity at ∼2 Hz [Fig. 12(b)]. However, the spectral differences between the shuffled and nonshuffled datasets were not significant ($P = 0.1738$). Finally, peripheral locations [Fig. 12(c)] around the future center of gaze ($\tan_{\text{peri-ccw+cw}}$, $\text{rad}_{\text{para+peri-in}}$, $\text{rad}_{\text{peri-out}}$) all exhibited rhythmicity at 2–3 Hz which, like in the foveal region, were statistically significantly different from location-shuffled data ($P = 0.0062$, 0.0071, and 0.0207, respectively).

Taken together, these results strongly suggest that attentional signals support changes in visual sensitivity in task-relevant regions of visual space around the current and future centers of gaze. However, at the intermediate parafoveal locations, the region of visual space susceptible to the incessant retinal disruptions saccades necessarily accompany, these changes in visual sensitivity are not strongly mediated by attentional signals. Concerning the proposed model, these results strongly suggest P_{RE} may be driven by attentional-oculomotor signals that are actively being mediated by delta rhythmicity.

IV. DISCUSSION

P_{RE} is a phenomenon actuated by cells across different retinotopic brain structures. This phenomenon has also been observed across different sensory modalities [16–20,89,90] and across foveated and afoveated biological systems [23,53]. Here, we were motivated by what is arguably the most puzzling question in the field of predictive remapping research [91]. Bruce and Goldberg [70] and Goldberg and Bruce [92] recapitulated translational effects observed in the superior colliculus by Mays and Sparks [37]. They found that, before the execution of a saccade, the receptive fields of cells in the frontal eye fields predictively shift their spatial extent beyond their classical extent toward their future fields (translational remapping). These neural effects were reproduced across several retinotopic brain structures including the lateral intraparietal area and extrastriate visual areas. Recapitulating in part the results of Tolias *et al.* [20], Zirnsak *et al.* [21] demonstrated that the receptive fields of cells in the frontal eye fields primarily converge around the attention-selected peripheral region of interest which included the spatial extent of the saccade target (convergent remapping).

We revisited these contradictory findings by introducing the Newtonian model of P_{RE} in which we proposed that the underlying presaccadic attentional and oculomotor signals

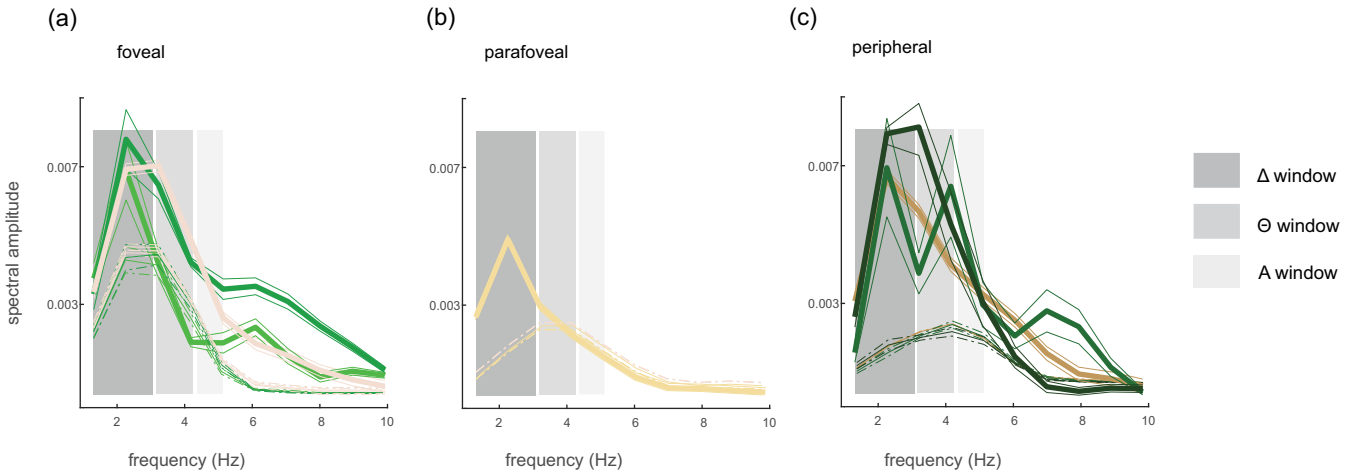

FIG. 12. Frequency domain representation of detrended visual sensitivity, unshuffled (solid lines), and shuffled (dotted lines, $n = 1500$) in the (a) fovea, (b) parafovea, and (c) periphery. The solid and dotted thinner solid lines represent the error estimates calculated across subjects.

manifest as temporally overlapping forces that act on retinotopic brain structures. Next, we systematically assessed the transient consequences of predictive remapping on visual sensitivity along and around the path of a saccade.

We show that, contrary to the dominant spatial account, predictive remapping is neither a purely convergent nor a translational phenomenon but rather one which must include a translational, convergent, and centripetal components. We demonstrate, contrary to the dominant restrictive account, predictive remapping is not limited to the current and future postsaccadic locations but includes intermediate parafoveal locations along the saccade trajectory within the early to midpresaccadic window [55]. This transiently shifts neural resources toward the current center of gaze that is eventually remapped toward the future center of gaze. Finally, we show that, contrary to the dominant temporal account of predictive remapping, centripetal shifts toward the fovea precede and overlap with convergent shifts toward the peripheral region of interest, while translational shifts parallel to the saccade trajectory occur later in time and overlap with convergent shifts.

In this paper, we make four principal contributions to a deeper understanding of predictive remapping. First, recipient retinotopic brain structures receive temporally overlapping inputs that align with a canonical order of presaccadic events. Second, the neural computations that underlie predictive remapping obey an inverse distance law. Third, during active sensing (when not in a state of equilibrium) RF_i very likely possesses putative transient eccentricity-dependent elastic fields (elφ's). It is likely that elφ's are self-generated by the visual system and allow these receptive fields to undergo a remarkable degree of elasticity beyond their classical spatial extent. Simulation results show, in the absence of these elφ's, orderly perception of the visual world would be dramatically distorted, as retinotopic cells would overcommit to certain loci in visual space at the expense of others which would compromise the ability to detect changes that occur in the peripheral region of visual space [6,84]. Finally, in this paper, we strongly suggest that the immediate availability of neural resources after the execution of a saccadic eye movement is uniquely mediated by centripetal signals directed toward the current center of gaze. Indeed, without centripetal signals or elφ's, attentional resources that are needed at the approximated location of the target would be significantly delayed and in the extreme case nonexistent [Fig. 9(d)].

V. CONCLUSIONS

In conclusion, we propose a simple, elegant, yet powerful mathematical framework that was implemented by the proposed model [93]. This framework uncovers a fundamental law and the functional architecture that mediates predictive remapping, which had eluded the field for decades. Akin to a successful model of neural remapping which a similar approach was used [94], this model not only offers critical insights that will inform future investigations of this phenomenon, specifically those concerned with uncovering the functional and neurobiological basis of elφ's, but also a powerful tool that experimentalists can now use to generate predictions across different types of biological systems.

ACKNOWLEDGMENTS

Thank you to Arnivan Nandy and Zixuan Xiao for helping with the experimental phase of this project, as well as former and current colleagues for their helpful discussions and comments, and finally, a special thanks to Michael Scudder for implementing the experimental design.

[1] J. Gottlieb and P. Y. Oudeyer, Towards a neuroscience of active sampling and curiosity, Nat. Rev. Neurosci. **19**, 758 (2019).

[2] F. Kano and J. Call, Great apes generate goal-based action predictions: An eye-tracking study, Psychol. Sci., **25**, 1691 (2014).

[3] S. H. Zahler, D. E. Taylor, J. Y. Wong, J. M. Adams, and E. H. Feinberg, Superior colliculus drives stimulus-evoked directionally biased saccades and attempted head movements in head-fixed mice, eLife **10**, e73081 (2021).

[4] L. M. Fenk, S. C. Avritzer, J. L. Weisman, A. Nair, L. D. Randt, T. L. Mohren, I. Siwanowicz, and G. Maimon, Muscles that move the retina augment compound eye vision in Drosophila, Nature (London) **10**, 116 (2022).

[5] S. E. Brockerhoff, Measuring the optokinetic response of zebrafish larvae, Nat. Protoc. **1**, 2448 (2006).

[6] I. E. Smart, I. C. Cuthill, and N. E. Scott-Samuel, In the corner of the eye: Camouflaging motion in the peripheral visual field, Proc. R. Soc. B **287**, 20192537 (2020).

[7] S. Mathôt and J. Theeuwes, Visual attention and stability, Phil. Trans. R. Soc. B **366**, 516 (2011).

[8] A. F. Meyer, J. O'Keefe, and J. Poort, Two distinct types of eye-head coupling in freely moving mice, Curr Biol. **30**, 2116 (2020).

[9] B. Cellini and J. M. Mongeau, Active vision shapes and coordinates flight motor responses in flies, Proc. Natl. Acad. Sci. USA **117**, 23085 (2020).

[10] M. Land, Eye movements in man and other animals, Vision Res. **162**, 1 (2019).

[11] H. V. Helmholtz, *A Treatise on Physiological Optics* (Dover, New York, 1962).

[12] E. von Holst and H. Mittelstaedt, The reafferent principle: Reciprocal effects between central nervous system and periphery, Naturwissenschaften **37**, 464 (1950).

[13] L. Stark and B. Bridgeman, Role of corollary discharge in space constancy, Percept. Psychophys. **34**, 371 (1983).

[14] W. P. Medendorp, Spatial constancy mechanisms in motor control, Philos. Trans. R. Soc. B **366**, 476 (2011).

[15] H. Deubel, B. Bridgeman, and W. X. Schneider, Immediate post-saccadic information mediates space constancy, Vision Res. **38**, 3147 (1998).

[16] J. R. Duhamel, C. L. Colby, and M. E. Goldberg, The updating of the representation of visual space in parietal cortex by intended eye movements, Science **255**, 90 (1992).

[17] M. F. Walker, E. J. Fitzgibbon, and M. E. Goldberg, Neurons in the monkey superior colliculus predict the visual result of impending saccadic eye movements, Neurophysiol. **73**, 1988 (1995).

[18] M. A. Sommer and R. H. Wurtz, Influence of the thalamus on spatial visual processing in frontal cortex, Nature (London) **444**, 374 (2006).

[19] K. Nakamura and C. L. Colby, Updating of the visual representation in monkey striate and extrastriate cortex during saccades, Proc. Natl Acad. Sci. USA **99**, 4026 (2002).

[20] A. S. Tolias, T. Moore, S. M. Smirnakis, E. J. Tehovnik, A. G. Siapas, and P. H. Schiller, Eye movements modulate visual receptive fields of V4 neurons, Neuron **29**, 757 (2001).

[21] M. Zirnsak, N. A. Steinmetz, B. Noudoost, K. Z. Xu, and T. Moore, Visual space is compressed in prefrontal cortex before eye movements, Nature (London) **507**, 504 (2014).

[22] T. S. Hartmann, M. Zirnsak, M. Marquis, F. H. Hamker, and T. Moore, Two types of receptive field dynamics in area V4 at the time of eye movements? Front. Syst. Neurosci. **11**, 13 (2017).

[23] S. D. Wiederman, J. M. Fabian, J. R. Dunbier, and D. C. O'Carroll, A predictive focus of gain modulation encodes target trajectories in insect vision, eLife **6**, e26478 (2017).

[24] M. Zirnsak and T. Moore, Saccades and shifting receptive fields: Anticipating consequences or selecting targets?, Trends Cogn. Sci. **18**, P621 (2014).

[25] J. D. Golomb and J. A. Mazer, Visual remapping, Annu. Rev. Vis. Sci. **7**, 257 (2021).

[26] P. Cavanagh, A. R. Hunt, A. Afraz, and M. Rolfs, Visual stability based on remapping of attention pointers, Trends Cogn. Sci. **14**, 147 (2010).

[27] S. Neupane, D. Guitton, and C. C. Pack, Perisaccadic remapping: What? How? Why? Rev. Neurosci. **31**, 505 (2020).

[28] K. Arkesteijn, A. V. Belopolsky, J. Smeets, and M. Donk, The limits of predictive remapping of attention across eye movements, Front. Psychol. **10**, 1146 (2019).

[29] M. Zirnsak, R. G. K. Gerhards, R. Kiani, M. Lappe, and F. H. Hamker, Anticipatory saccade target processing and the presaccadic transfer of visual features, J. Neurosci. **31**, 17887 (2011).

[30] M. Rolfs, D. Jonikaitis, H. Deubel, and P. Cavanagh, Predictive remapping of attention across eye movements, Nat. Neurosci. **14**, 252 (2011).

[31] M. Szinte, D. Jonikaitis, D. Rangelov, and H. Deubel, Presaccadic remapping relies on dynamics of spatial attention, eLife **7**, e37598 (2018).

[32] S. Neupane, D. Guitton, and C. C. Pack, Two distinct types of remapping in primate cortical area V4, Nat. Commun. **7**, 10402 (2016).

[33] S. Neupane, D. Guitton, and C. C. Pack, Dissociation of forward and convergent remapping in primate visual cortex, Curr. Biol. **26**, R491 (2016).

[34] M. H. Phillips and J. A. Edelman, The dependence of visual scanning performance on saccade, fixation, and perceptual metrics, Vision Res. **48**, 926 (2008).

[35] M. T. Wong-Riley, Energy metabolism of the visual system, Eye Brain **2**, 99 (2010).

[36] T. Yao, M. Ketkar, S. Treue, and B. S. Krishna, Visual attention is available at a task-relevant location rapidly after a saccade, eLife **5**, e18009 (2016).

[37] L. E. Mays and D. L. J. Sparks, Dissociation of visual and saccade-related responses in superior colliculus neurons, Neurophysiol. **43**, 207 (1980).

[38] A. Bozis and A. K. Moschovakis, Neural network simulations of the primate oculomotor system. III. A one-dimensional, one-directional model of the superior colliculus, Biol. Cybern. **79**, 215 (1998).

[39] S. Deneve, J. R. Duhamel, and A. Pouget, Optimal sensorimotor integration in recurrent cortical networks: A neural implementation of Kalman filters, J. Neurosci. **27**, 5744 (2007).

[40] J. Xing and R. A. Andersen, Memory activity of LIP neurons for sequential eye movements simulated with neural networks, J. Neurophysiol. **84**, 651 (2000).

[41] K. Krommenhoek, A. Van Opstal, C. Gielen, and J. Van Gisbergen, Remapping of neural activity in the motor colliculus: A neural network study, Vision Res. **33**, 1287 (1993).

[42] C. Quaia, L. M. Optican, and M. E. Goldberg, The maintenance of spatial accuracy by the perisaccadic remapping of visual receptive fields, Neural Netw. **11**, 1229 (1998).

[43] H. M. Rao, J. San Juan, F. Y. Shen, J. E. Villa, K. S. Rafie, and M. A. Sommer, Neural network evidence for the coupling of presaccadic visual remapping to predictive eye position updating, Front. Comput. Neurosci. **10**, 52 (2016).

[44] J. Droulez and A. Berthoz, A neural network model of sensoritopic maps with predictive short-term memory properties, Proc. Natl. Acad. Sci. USA **88**, 9653 (1991).

[45] G. P. Keith, G. Blohm, and J. D. Crawford, Influence of saccade efference copy on the spatiotemporal properties of remapping: A neural network study, J. Neurophysiol. **103**, 117 (2010).

[46] M. Zirnsak, M. Lappe, and F. H. Hamker, The spatial distribution of receptive field changes in a model of peri-saccadic perception: Predictive remapping and shifts towards the saccade target, Vision Res. **50**, 1328 (2010).

[47] R. B. Laughlin, *A Different Universe: Reinventing Physics from the Bottom Down* (Basic Books, New York, 2005).

[48] H. K. Hartline, The receptive fields of optic nerve fibers, Am. J. Physiol. **130**, 690 (1940).

[49] D. H. Hubel and T. N. Wiesel, Receptive fields and functional architecture of monkey striate cortex, J. Physiol. **195**, 215 (1968).

[50] N. C. Klapoetke, A. Nern, E. M. Rogers, G. M. Rubin, M. B. Reiser, and G. M. Card, A functionally ordered visual feature map in the Drosophila brain, Neuron **110**, P1700 (2022).

[51] S. C. Yang, D. M. Wolpert, and M. Lengyel, Theoretical perspectives on active sensing, Curr. Opin. Behav. Sci. **11**, 100 (2018).

[52] A. Filosa, A. J. Barker, M. Dal Maschio, and H. Baier, Feeding state modulates behavioral choice and processing of prey stimuli in the zebrafish tectum, Neuron **90**, 596 (2016).

[53] I. B. Witten, J. F. Bergan, and E. L. Knudsen, Dynamic shifts in the owl's auditory space map predict moving sound location, Nat. Neurosci. **9**, 1439 (2006).

[54] J. Moran and R. Desimone, Selective attention gates visual processing in the extrastriate cortex, Science **229**, 782 (1985).

[55] X. Wang, C. C. A. Fung, S. Guan, S. Wu, M. E. Goldberg, and M. Zhang, Perisaccadic receptive field expansion in the lateral intraparietal area, Neuron **90**, 400 (2016).

[56] Y. T. Li, L. A. Ibrahim, B.-h. Liu, L. I. Zhang, and H. W. Tao, Linear transformation of thalamocortical input by intracortical excitation, Nat. Neurosci. **16**, 1324 (2013).

[57] Z. M. Hafed, Alteration of visual perception prior to microsaccades, Neuron **77**, 775 (2013).

[58] H. M. Rao, J. P. Mayo, and M. A. Sommer, Circuits for presaccadic visual remapping, J. Neurophysiol. **116**, 2624 (2016).

[59] M. Kaiser and M. Lappe, Perisaccadic mislocalization orthogonal to saccade direction, Neuron **41**, 293 (2004).

[60] E. Zimmermann, M. C. Morrone, and D. C. Burr, Visual mislocalization during saccades sequences, Exp. Brain Res. **233**, 577 (2014).

[61] J. Ross, M. C. Morrone, and D. C. Burr, Compression of visual space before saccades, Nature (London) **386**, 598 (1997).

[62] S. Idrees, M. P. Baumann, F. Franke, T. A. Münch, and Z. M. Hafed, Perceptual saccadic suppression starts in the retina, Nat. Commun. **11**, 1977 (2020).

[63] Z. M. Hafed and J. J. Clark, Microsaccades as an overt measure of covert attention shifts, Vision Res. **42**, 2533 (2002).

[64] M. Juusola, A. Dau, Z. Song, N. Solanki, D. Rien, D. Jaciuch, S. A. Dongre, F. Blanchard, G. G. de Polavieja, R. C. Hardie *et al.*, Microsaccadic sampling of moving image information provides Drosophila hyperacute vision, eLife. **6**, e26117 (2017).

[65] C. D. Holmgren, P. Stahr, D. J. Wallace, K.-M. Voit, E. J. Matheson, J. Sawinski, G. Bassetto, and J. N. D. Kerr, Visual pursuit behavior in mice maintains the pursued prey on the retinal region with least optic flow, eLife. **10**, e70838 (2021).

[66] A. M. Michaiel, E. T. Abe, and C. M. Niell, Dynamics of gaze control during prey capture in freely moving mice, eLife **9**, e57458 (2020).

[67] C. A. Bosman, T. Womelsdorf, R. Desimone, and P. Fries, A microsaccadic rhythm modulates gamma-band synchronization and behavior, J. Neurosci. **29**, 9471 (2009).

[68] D. P. Munoz and R. H. Wurtz, Saccade-related activity in monkey superior colliculus. I. Characteristics of burst and build-up neurons, J. Neurophysiol. **73**, 2313 (1995).

[69] M. A. Sommer and R. H. Wurtz, What the brain stem tells the frontal cortex. II. Role of the SC-MD-FEF pathway in corollary discharge, J. Neurophysiol. **91**, 1403 (2004).

[70] D. J. Bruce and M. E. Goldberg, Primate frontal eye fields. I. Single neurons discharging before saccades, J. Neurophysiol. **53**, 603 (1985).

[71] L. M. Heiser and C. L. Colby, Spatial updating in area LIP is independent of saccade direction, J. Neurophysiol. **95**, 2751 (2006).

[72] A. J. van Opstal, K. Hepp, B. J. M. Hess, D. Straumann, and V. Henn, Two- rather than three-dimensional representation of saccades in monkey superior colliculus, Science **252**, 1313 (1991).

[73] R. M. Pritchard, Stabilized images on the retina, Sci. Am. **204**, 72 (1961).

[74] C. Y. Chen, K. P. Hoffmann, C. C. Distler, and Z. M. Hafed, The foveal visual representation of the primate superior colliculus, Curr. Biol. **29**, 2109 (2019).

[75] M. Carrasco, D. L. Evert, I. Chang, and S. M. Katz, The eccentricity effect: Target eccentricity affects performance on conjunction searches, Percept. Psychophys. **57**, 1241 (1995).

[76] E. Matin, Saccadic suppression: A review and an analysis, Psychol. Bull. **81**, 899 (1974).

[77] See Supplemental Material at http://link.aps.org/supplemental/10.1103/PhysRevResearch.5.013214 for simulated heatmaps, approximating population neural activity before a saccade, shows the importance of the centripetal, convergent and translational components of predictive remapping.

[78] R. N. Gutenkunst, J. J. Waterfall, F. P. Casey, K. S. Brown, C. R. Myers, and J. P. Sethna, Universally sloppy parameter sensitivities in systems biology models, PLoS Comput. Biol. **3**, 1871 (2007).

[79] C. Stringer, M. Michaelos, D. Tsyboulski, S. E. Lindo, and M. Pachitariu, High-precision coding in visual cortex, Cell **184**, 2767 (2021).

[80] C. Stringer, M. Pachitariu, N. Steinmetz, C. B. Reddy, M. Carandini, and K. D. Harris, Spontaneous behaviors drive multidimensional brain wide activity, Science **364**, 255 (2019).

[81] C. Stringer, M. Pachitariu, N. Steinmetz, M. Carandini, and K. D. Harris, High-dimensional geometry of population responses in visual cortex, Nature (London) **571**, 361 (2019).

[82] J. A. Easterbrook, The effect of emotion on cue utilization and the organization of behavior, Psychol. Rev. **66**, 183 (1959).

[83] K. C. Mills, S. E. Spruill, R. W. Kanne, K. M. Parkman, and Y. Zhang, The influence of stimulants, sedatives, and fatigue on tunnel vision: Risk factors for driving and piloting, Hum. Factors **43**, 310 (2001).

[84] M. P. S. To, B. C. Regan, D. Wood, and J. D. Mollon, Vision out of the corner of the eye, Vision Res. **51**, 203 (2011).

[85] I. C. Fiebelkorn, Y. B. Saalmann, and S. Kastner, Rhythmic sampling within and between objects despite sustained attention at a cued location, Curr. Biol. **23**, 2553 (2013).

[86] A. Benedetto and M. C. Morrone, Visual sensitivity and bias oscillate phase-locked to saccadic eye movements, J. Vis. **19**, 15 (2019).

[87] A. Benedetto and M. C. Morrone, Saccadic suppression is embedded within extended oscillatory modulation of sensitivity, J. Neurosci. **37**, 3661 (2017).

[88] H. Hogendoorn, Voluntary saccadic eye movements ride the attentional rhythm, J. Cogn. Neurosci. **28**, 1625 (2016).

[89] M. F. Jay and D. L. Sparks, Auditory receptive fields in primate superior colliculus shift with changes in eye position, Nature (London) **309**, 345 (1984).

[90] M. F. Jay and D. L. Sparks, Sensorimotor integration in the primate superior colliculus. II. Coordinates of auditory signals, J. Neurophysiol. **57**, 35 (1987).

[91] E. P. Merriam, C. R. Genovese, and C. L. Colby, Remapping in human visual cortex, J. Neurophysiol. **97**, 1738 (2007).

[92] M. E. Goldberg and C. J. Bruce, Primate frontal eye fields. III. Maintenance of a spatially accurate saccade signal, J. Neurophysiol. **64**, 489 (1990).

[93] I. E. Adeyefa-Olasupo, Retinotopic mechanics derived using classical physics, arXiv:2109.11632.

[94] S. A. Ocko, K. Hardcastle, L. M. Giocomo, and S. Ganguli, Emergent elasticity in the neural code for space, Proc. Nat. Acad. Sci. USA **115**, 50 (2018).